SUMMER DRYNESS DUE TO AN INCREASE OF ATMOSPHERIC CO_2 CONCENTRATION

S. MANABE, R. T. WETHERALD,
and
R. J. STOUFFER
Geophysical Fluid Dynamics Laboratory/NOAA, Princeton University, P. O. Box 308, Princeton, New Jersey 08540, U.S.A.

Abstract. To investigate the hydrologic changes of climate in response to an increase of CO_2-concentration in the atmosphere, the results from numerical experiments with three climate models are analyzed and compared with each other. All three models consist of an atmospheric general circulation model and a simple mixed layer ocean with a horizontally uniform heat capacity. The first model has a limited computational domain and simple geography with a flat land surface. The second model has a global computational domain with realistic geography. The third model is identical to the second model except that it has a higher computational resolution. In each numerical experiment, the CO_2-induced change of climate is evaluated based upon a comparison between the two climates of a model with normal and four times the normal concentration of carbon dioxide in air.

It is noted that the zonal mean value of soil moisture in summer reduces significantly in two separate zones of middle and high latitudes in response to the increase of the CO_2-concentration in air. This CO_2-induced summer dryness results not only from the earlier ending of the snowmelt season, but also from the earlier occurrence of the spring to summer reduction in rainfall rate. The former effect is particularly important in high latitudes, whereas the latter effect becomes important in middle latitudes. Other statistically significant changes include large increases in both soil moisture and runoff rate in high latitudes of a model during most of the annual cycle with the exception of the summer season. The penetration of moisture-rich, warm air into high latitudes is responsible for these increases.

1. Introduction

The change of climate due to an increase of atmospheric CO_2 has been studied through the use of general circulation models (e.g., Manabe and Wetherald, 1975, 1980). This study is an extension of the recent investigations by Manabe and Stouffer (1979, 1980) and Wetherald and Manabe (1981) which utilized numerical models of atmosphere-mixed layer ocean systems with realistic and idealized geography, respectively.

One of the topics discussed in both of these studies was the seasonal and latitudinal variation of the CO_2-induced changes of various hydrologic variables. However, it was difficult to discuss this aspect of the results with any degree of confidence for the following reasons.

(1) In the numerical time integration of the climate models, the hydrologic variables exhibit large temporal and spacial variations. Thus it was difficult to distinguish the signal of the CO_2-induced hydrologic change from the normal hydrologic fluctuation.

(2) The seasonal and geographical distribution of the hydrologic variables as simulated

Climatic Change 3 (1981) 347–386. 0165–0009/81/0034–0347$04.00.

by the model with realistic geography contains many unrealistic features partly due to the coarseness of the computational resolution of the model.

Since the publication of the study of Manabe and Stouffer (1980), the present authors have repeated their experiment by use of a global model with higher computational resolution. It was found that the hydrologic characteristics of the climate for this high resolution model is more realistic than the corresponding features of climate described by Manabe and Stouffer. However, the CO_2-induced climate change obtained from this latest model includes many features which are shared by the corresponding changes from the other two studies discussed above. This study attempts to develop a consensus scenario for the CO_2-induced change of hydrologic variables based upon a comparative analyses of the results from the three models, i.e., (1) the model with idealized geography, (2) the global model with realistic geography and relatively low computational resolution, and (3) the global model with relatively high computational resolution.

2. Model Structure and Numerical Time Integration

The mathematical model used for this study, as shown schematically by Figure 1, consists of three basic units: (1) a general circulation model of the atmosphere, (2) a heat and water balance model over the continents, and (3) a simple model of the mixed layer in the oceans. A description of these three units follows.

The general circulation model of the atmosphere computes the changes in the vertical component of vorticity, horizontal divergence, temperature, moisture, and surface pressure based upon the equations of motion, the thermodynamical equation and the continuity equations for moisture and mass. The horizontal distributions of the variables are represented by a finite number of spherical harmonics. The model computes the rates of change of a prognostic variable at all grid points and transforms them back to spectral domain as suggested by Orsag (1970). The horizontal resolution of a spectral model is

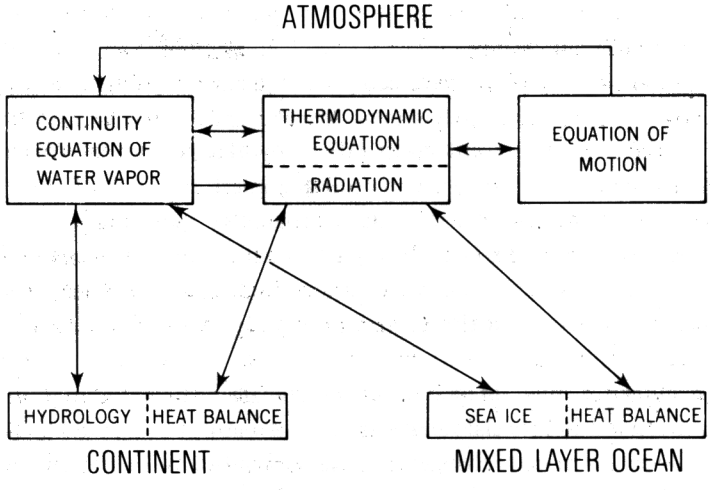

Fig. 1. Box diagram illustrating the basic structure of the mathematical model of climate.

determined by the number of spectral components retained. In the present study, the number of components, which are retained in both zonal and meridional directions, are fifteen or twenty-one depending on the version of the model used. The vertical derivatives in the prognostic equation are computed by a finite difference method. The model has nine unevenly-spaced finite difference levels.

The prognostic equations are numerically integrated in time by a semi-implicit method. In this method, the linear and non-linear components of the rate of change of a variable are separated and time integrated implicitly and explicitly, respectively.

The basic structure of the dynamical component described above was developed by Gordon and Stern (1974) and it is very similar to the spectral model developed by Bourke (1974) and Hoskins and Simmons (1975). The reader is referred to their papers for more details. Also, the relative performance of different resolutions of this general circulation model of the atmosphere are described by Manabe *et al.* (1979).

The distribution of the incoming solar radiation is prescribed at the top of the atmosphere. The method for the computation of solar radiation flux is similar to the one described by Lacis and Hansen (1974). For simplicity, diurnal variation is removed. Terrestrial radiation is computed by the method which was developed by Rogers and Walshaw (1966) and modified by Stone and Manabe (1968). For the computation of both the solar and terrestrial radiation fluxes the effects due to carbon dioxide, ozone, water vapor and cloud cover are taken into consideration. The mixing ratio of carbon dioxide is assumed to be constant everywhere. Ozone is specified as a function of latitude, height, and season. Cloud cover is prescribed to be zonally uniform and invariant with respect to season. The water vapor distribution is determined by the prognostic equations.

Precipitation is predicted whenever supersaturation is indicated by the prognostic equation for water vapor. Snowfall is forecast when the air temperature near the surface falls below freezing; otherwise rain is predicted. The moist convection processes are incorporated by a moist convective adjustment scheme. See Manabe *et al.* (1965) for more details.

The temperature of the continental surface is computed so that it satisfies the condition of local thermal equilibrium at the surface. The soil albedo, which is needed to determine the net solar flux at the ground, is prescribed geographically based upon a study by Posey and Clapp (1964). It is replaced by a larger albedo in snow-covered areas. A change in the snow depth is predicted as the net contribution from snowfall, sublimation, and snowmelt which is determined from the surface heat budget.

The ground water budget is computed by the so-called bucket method. In the present study, the field capacity of the soil is assumed to be 15 cm. If the soil moisture value exceeds the field capacity, runoff is predicted. A change of soil moisture is computed from the rates of rainfall, evaporation, snowmelt and runoff. The rate of evaporation from soil surface is determined as a function of soil moisture and the potential evaporation rate (i.e., the hypothetical evaporation rate from a completely wet soil). See Manabe (1969) for further details of the hydrologic computations over the continental surface.

The mixed layer model of the oceans is a vertically isothermal layer of sea water 68.5 m deep. Its thickness is chosen to yield approximately the observed seasonal amplitude of

the sea surface temperature. The time rate of change of the temperature in the ice free regions is computed from the net contribution of the solar and terrestrial radiation fluxes and the sensible and latent heat fluxes at the ocean surface. The effects of horizontal heat transport by ocean currents and that of the heat exchange between the mixed layer and the deeper layer of the ocean are neglected. In the presence of sea ice, the mixed layer temperature is fixed at the freezing point of sea water (−2 °C) and the heat conduction through the ice is balanced by the latent heat of freezing (melting) at the bottom of the ice layer. This process, together with the melting at the ice surface, sublimation and snowfall determine the change in the ice thickness (Bryan, 1969). For the computation of the net solar radiation at the oceanic surface, albedo is prescribed as a function of latitude. Over the regions covered by sea ice, higher values of albedo are used. For a more detailed description of the mixed layer ocean model, see Manabe and Stouffer (1980).

Table I summarizes the individual characteristics of three versions of the basic model which are used for this study. The first version i.e., the S15 model was originally used by Wetherald and Manabe (1981). It has an idealized flat geography and a 'sector' computational domain illustrated in Figure 2. The notation 'S' indicates the sector domain while '15' identifies the maximum zonal wave number of the retained spectral components. To insure the cyclic continuity of model variables between the two boundary meridians, every third zonal wave component is retained in this model. The second version i.e., the G15 model was originally used by Manabe and Stouffer (1979, 1980). It has a global computational domain and realistic geography. Again, the maximum zonal wave number of the retained components is 15. The third version i.e., the G21 model is introduced in the present study. It is identical to the G15 model except that it has a higher computational resolution. The maximum zonal wave number is 21 for this model.

The economical time integration method used to achieve a statistically stationary climate of a model is similar to the method described by Manabe and Stouffer (1980) and Wetherald and Manabe (1981). Refer to their papers for the details of this method. Starting from an isothermal initial condition (at 290 °K), the time integration of the S15- and G15-model are performed over periods of 20 and 15 yrs, respectively. For economy of computer time, the G21 model integration is started from the final equilibrium state from the G15 model integration and continued over a period of 5 yrs.

Towards the end of each time integration, a version of the model reaches a statistically stationary state. Therefore, the final several year period from each integration is chosen

TABLE I. Individual characteristics of the three versions of the model used for the present study

Version	Domain	Geography	Maximum zonal wave numbers	Length of time-integration (yrs)	Length of analysis period (yrs)
S15	Sector	Idealized	15	20	4 × 2 = 8
G15	Global	Realistic	15	13	3
G21	Global	Realistic	21	13 + 5	3

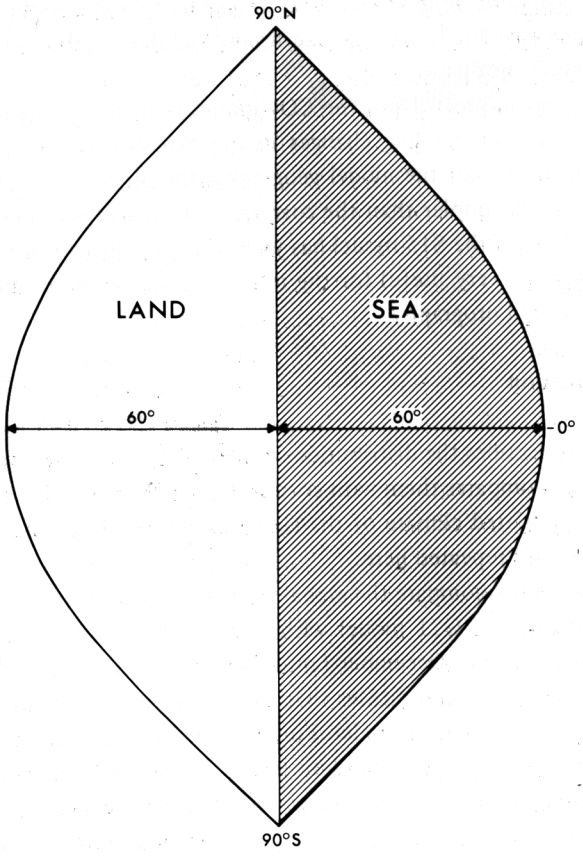

Fig. 2. Computational domain of the S15 model.

for an extensive analysis. The length of this analysis period is 4 yrs for the S15 model while it is 3 yrs for both the G15- and G21-models. It should be noted here, that, for the S15 model, the results from two symmetric hemispheres yield an effective 8 yr period for the analysis.

All three versions of the basic model are time-integrated with a normal (300 ppm*) and four times the normal (1200 ppm) values of the concentration of carbon dioxide in the atmosphere. These two cases will be referred to as the standard and 4 x CO_2-experiments, respectively. By comparing the difference between the 4 x CO_2- and standard climates from the 3 versions of the basic model, the hydrologic influence of the increase of carbon dioxide concentration will be investigated. The increase in CO_2 concentration is deliberately chosen to be large as compared with any foreseeable change of atmospheric CO_2 in order to discriminate the CO_2-induced change from background temporal fluctuation of a model climate. The CO_2-climate sensitivity study, which was conducted recently by Manabe and Wetherald (1980) using a sector model, indicates that

* Parts per million by volume.

the change of atmospheric temperature due to a CO_2-doubling is about half as large as the corresponding change due to a CO_2-quadrupling and the distributions of these changes are very similar to one another.

This study explores in great detail the CO_2-induced change of the S15 model climate before evaluating the corrsponding changes in the climates of the two global models. Because of the idealization of the model geography, the geographical features of a sector model climate are much simpler than the corresponding features from the global models. Therefore, the analysis of the S15 model has yielded a basic insight into the CO_2-induced change of climate and is very useful for the interpretation of the results from the global models with complicated orography.

3. Standard Simulation

This section briefly describes the distributions of some key hydrologic variables simulated by these models and compares them with corresponding observed distributions. Since the description of the simulated climate of the G15 model was already made by Manabe and Stouffer (1980), it is not repeated here.

Figures 3a, b, 4a, and b compare the global distributions of precipitation rate from the standard experiment of the G21 model with the corresponding observed distributions (Möller, 1951) for both the December-January-February (DJF) and June-July-August (JJA) seasons. This comparison indicates that many features of the observed DJF distribution are reproduced by the G21 model. For example, the tropical rainbelt is computed to be in approximately its observed position just south of the equator although there is no separate branch on the north side of the equator. The continental distributions of precipitation rate over South America, Australia, Africa and the United States are also approximately reproduced although the model overestimates the precipitation rate over the United States. In particular, the low precipitation rate over the Sahara Desert region is well simulated during this season. Prominent discrepancies include too much precipitation in middle to high latitudes in the Northern Hemisphere and a southward displacement of the Pacific and Atlantic oceanic rainbelts as compared to observation. However, the precipitation rates over continents in middle to higher latitudes of the Northern Hemisphere are not as excessive as they were for the G15 model (see Manabe and Stouffer, 1980).

The simulation in low latitudes for the JJA season is worse than that for the DJF season. In particular, the tropical rainbelt of the G21 model over both the tropical Pacific and Atlantic Ocean is located to the south of the equator in disagreement with the observed characteristics. As is the case with respect to the G15 model simulation (Manabe and Stouffer, 1980), the sea surface temperature over the Southern Hemisphere of the G21 model is generally too high and is probably responsible for the unrealistic placement of the tropical rainbelt. The comparison between Figures 4a and b also indicates that the precipitation rate is too small over southeast Asia and India and is too large to the south of the equator in South America of the model. It is probable that these unrealistic features are related to the bias of the model to form the tropical rainbelt to the south of the

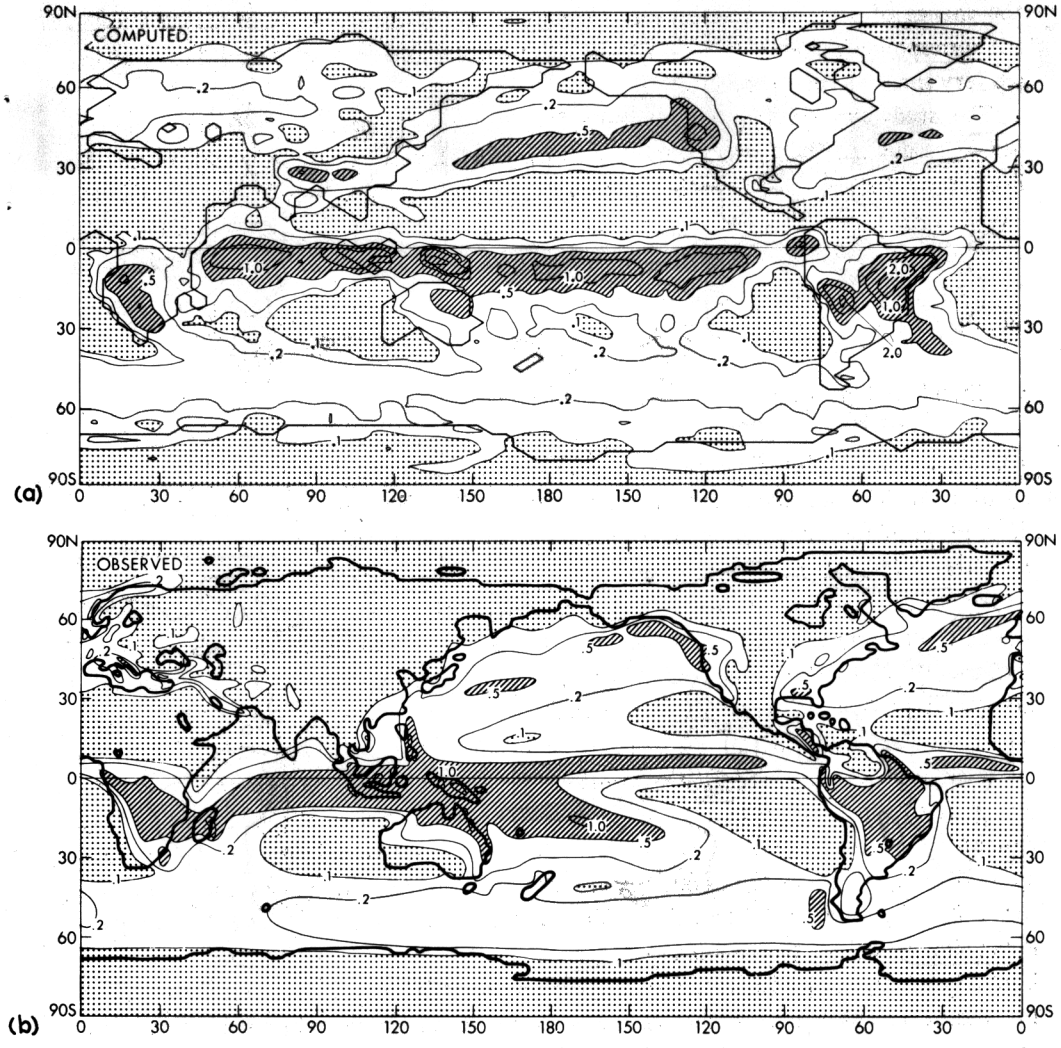

Fig. 3. Geographical distribution of December-January-February mean precipitation rate (cm/day). Top: the G21 model. Bottom: observation (Möller, 1959). Slanted shade indicates the area where the precipitation rate exceeds 0.5 cm/day, whereas dotted shade denotes the area where it is below 0.1 cm/day.

equator. Despite these differences, the G21 model reproduces the areas of relatively low precipitation rate over the Sahara, South African, Australian and central Asian deserts in the JAA distribution of the observed precipitation rate. Furthermore, the computed JJA distribution also compares favorably with the observed precipitation rates in middle and high latitudes.

Figures 5a and b compare the annual mean distribution of runoff rate for the G21 model with the corresponding observed distribution (Lvovitch and Ovlchinnikov, 1964). In general, the computed distribution of runoff rate agrees reasonably well with obser-

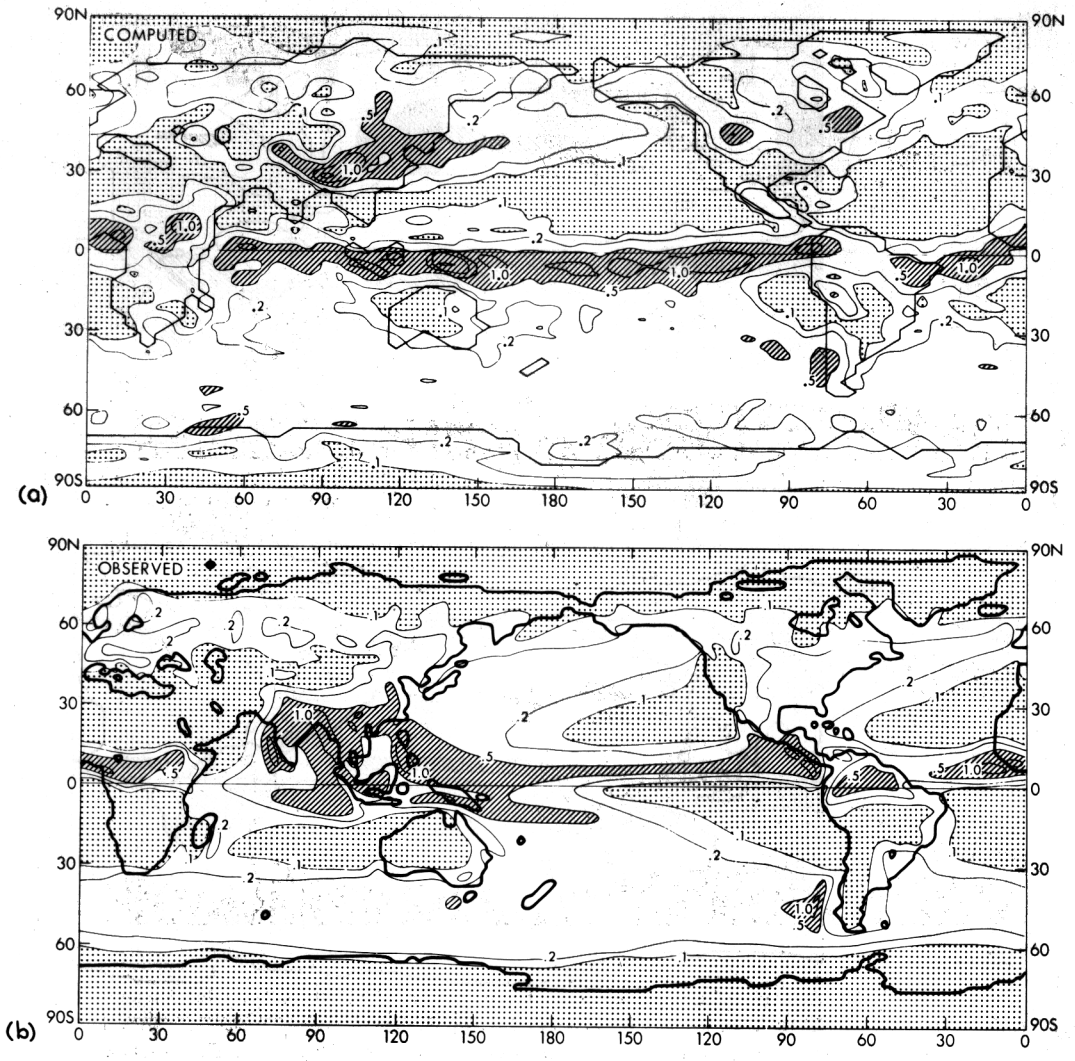

Fig. 4. Same as Figure 3 but for June-July-August.

vation in many areas such as Africa, northern and central Asia, Australia, and the western half of the United States. In particular, the major arid regions with a small runoff rate are reproduced by the model over the Sahara, Australian, and Central Asian deserts along with the southwestern United States. These arid regions are found to be more extensive for the G21 model as compared with the G15 model. This is consistent with the previous discussion on precipitation rates. Notable differences between the computed and the observed distributions are indicated over South America and southeastern Asia. The simulated runoff rate over the South American continent is too large south of the equator, whereas it is too small north of the equator, and over southeastern Asia. The reason for these differences is connected with the computed position of the tropical rainbelt, as

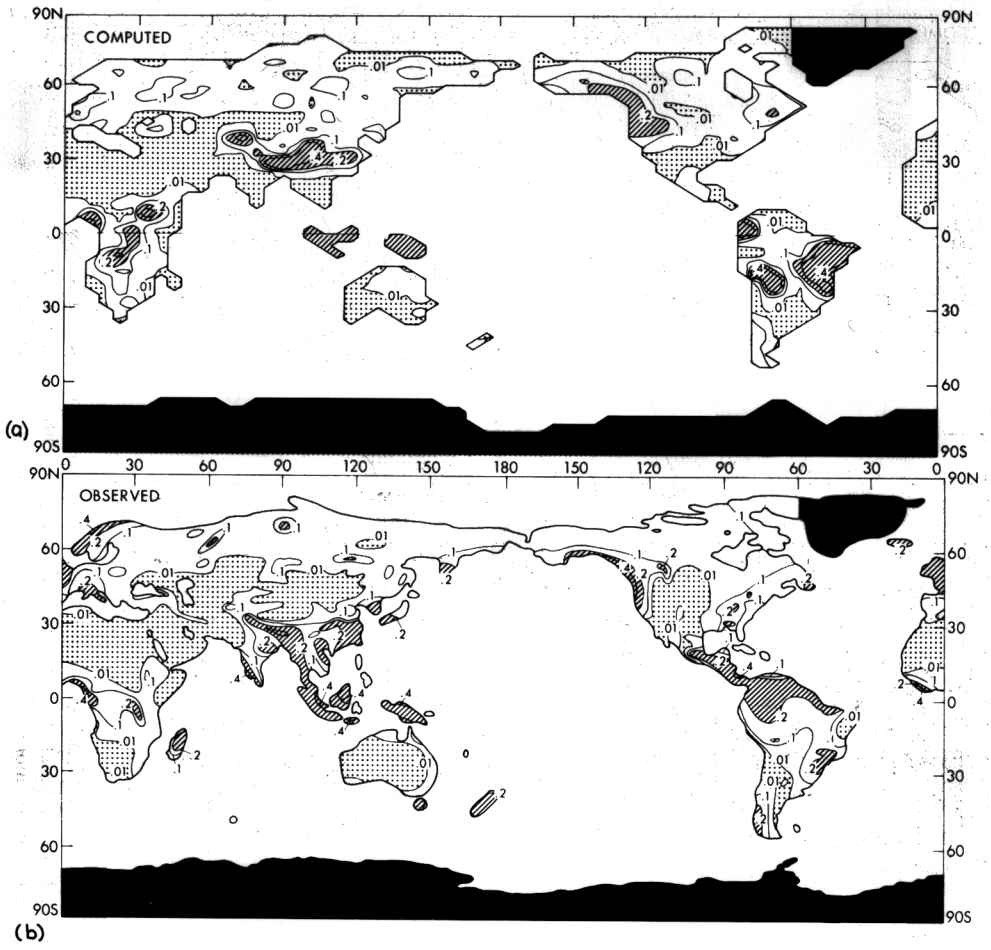

Fig. 5. Geographical distribution of annual mean runoff rate (cm/day). Top: the G21 model. Bottom: observation (Lvovitch and Ovtchennikov, 1964). Slanted shade indicates the area where the runoff rate exceeds 0.2 cm/day, whereas dotted shade denotes the area below 0.01 cm/day. The observed distribution shown here is an approximate copy of the original map.

mentioned earlier. In the higher latitudes, the computed runoff rate over northwestern Europe is too small in comparison with observation.

Since the results from the sensitivity study with the S15 model are extensively discussed in this study, it is worthwhile to compare the winter and summer distributions of precipitation rates obtained from this model (Figures 6a and b) with the observed distributions. In view of the highly idealized geography of the S15 model, one can make only very general comparisons. For example, one may identify in the winter S15 distribution an oceanic tropical rainbelt, a subtropical dry zone, and the mid-latitude rainbelt centered at about 45° latitude. In addition, one may note a narrow meridional belt of relatively large precipitation rate along the east coast of the subtropical portion of the idealized model continent. Turning to the summer S15 distribution, one may note similar features

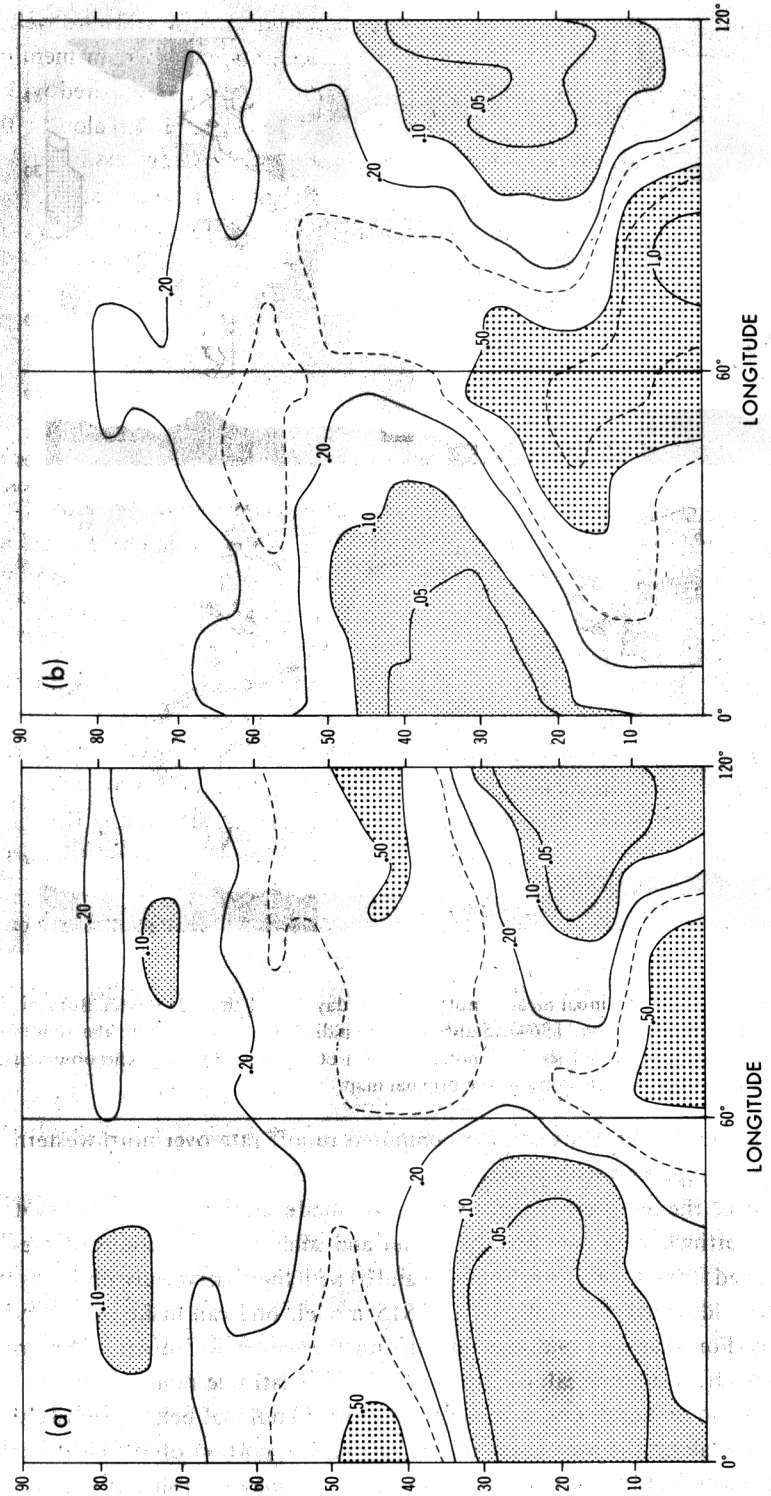

Fig. 6. Geographical distrbution of 3-monthly mean precipitation rate (cm/day) obtained from the S15 model for (a) the winter season and (b) the summer season. The rule for shading is the same as that used for Figure 3. The distributions of the two hemispheres of the model averaged after shifting the phase of the seasonal variation of the southern hemisphere precipitation rate by six months.

though the tropical rainbelt is considerably more intense and extends westward well into the continent in a monsoon pattern. The coastal precipitation maximum mentioned above is also more intense and extends more into higher latitudes as compared with the DJF distribution. The subtropical dry zone has extended poleward as well along with an accompanying poleward shift of the midlatitude rainbelt which is now less intense and centered at about 60° latitude. One can identify qualitatively similar features in the observed DJF and JJA distributions. In summary, the S15 model succeeds in simulating many of the gross features of the observed precipitation patterns in the real atmosphere despite the simplicity of the continental and oceanic shape adopted.

4. Hydrologic Response

4.1. Zonal mean distribution

As explained earlier, this section begins with the discussion of the results from the S15 model. Figure 7a illustrates the latitude-time distribution of the difference in zonal mean soil moisture over the continent between the 4 x CO_2- and the standard experiments obtained from the S15 model. For reference, the corresponding distribution of zonal mean soil moisture from the standard experiment is shown in Figure 7b.

According to Figure 7a, the difference of the zonal mean soil moisture in high latitudes of the S15 model has a large positive value throughout most of the year except for summer. As discussed by Manabe and Wetherald (1980), this CO_2-induced increase results from the enhancement of the poleward moisture transport. Figure 7a also indicates two distinct zones of reduced soil wetness in middle and high latitudes during the summer season. This CO_2-induced summer dryness is the main topic for the present study. Because of this increased dryness in middle latitudes, the subtropical dry zone (indicated in Figure 7b) extends polewards by about 5° of latitude during summer in response to the quadrupling of the atmospheric CO_2-concentration.

To appreciate the relative magnitude of soil moisture changes described above, the percentage change of zonal mean soil moisture is computed and shown in Figure 7c. (Here, the percentage change is defined as $100 \times \Delta[w]/[w]$ where w is soil moisture, [ ] indicates a zonal mean, operator over the continents, and Δ indicates the difference between the 4 x CO_2- and standard experiments. In this case, $[w]$ is computed from the results of the standard experiment.)

Figure 7c indicates that, during summer, the percentage reduction of zonal mean soil moisture ranges from 20 to 60% around 50° latitude and from 10 to 40% around 70° latitude. The percentage increase of zonal mean soil moisture, which occurs in high latitudes with the exception of the summer season, amounts to as much as 60%. In short, the change in zonal mean soil moisture described in the preceding paragraph constitutes a substantial fraction of the value of the soil moisture itself.

Although one also notes the zones of large percentage change of zonal mean soil moisture in both the subtropics and tropics of the S15 model, the change has relatively small statistical significance as discussed later.

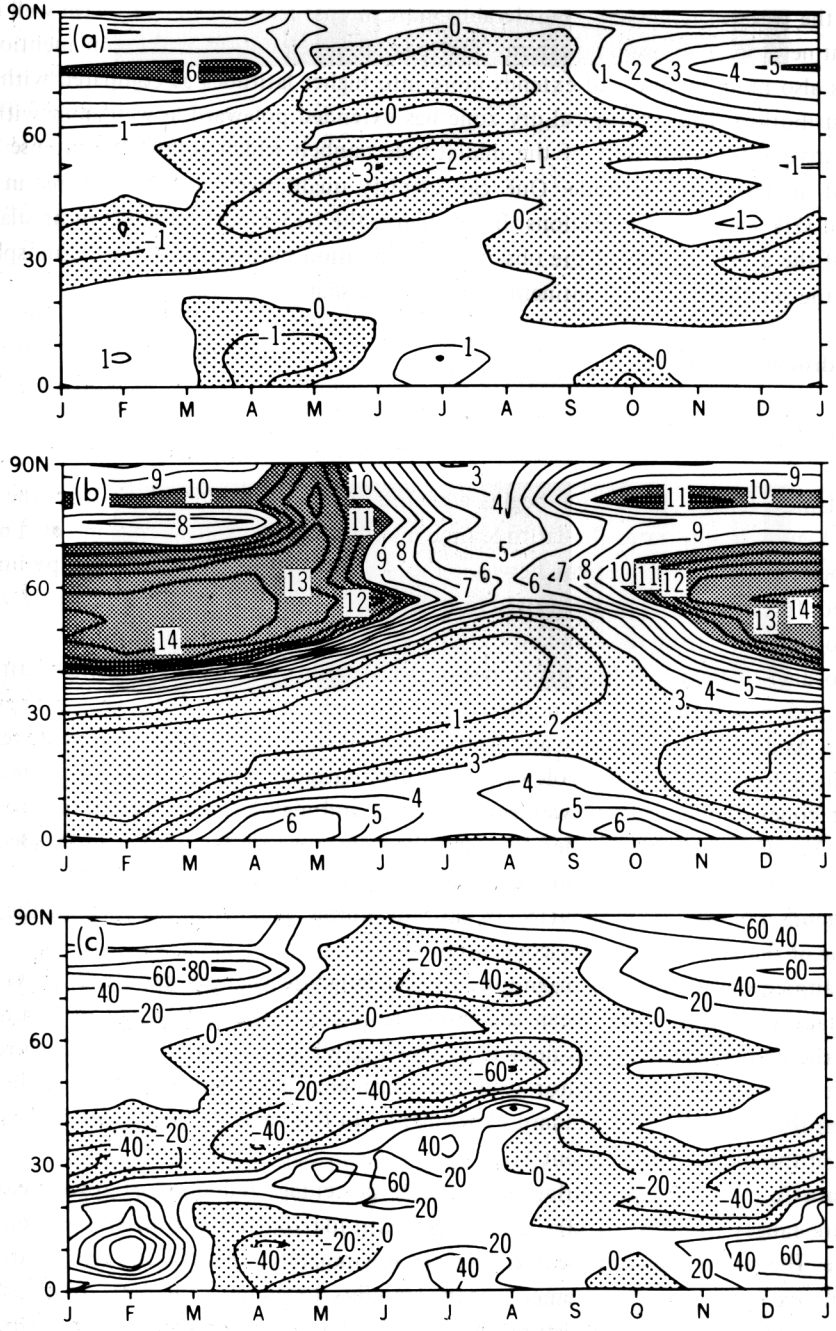

Fig. 7. The latitudinal and seasonal variation of the zonal mean (a) difference of soil moisture (cm) between the 4 x CO_2- and the standard experiments (same as Figure 17 of Wetherald and Manabe, 1981), (b) soil moisture (cm) for the standard experiment, and (c) percentage change of the soil moisture from the standard to the 4 x CO_2-experiments with the S15 model. The distribution of the two hemispheres of the model are averaged after shifting the timing of the southern hemisphere distribution by six months.

Examining Figures 8a and b which illustrate the latitude-time distributions of the CO_2-induced changes of zonal mean soil moisture from the G15- and G21-global models, one notes patterns which are qualitatively similar to those from the S15-model. For example, one can identify two zones of soil reduction in middle and high latitudes during summer, though the two zones are placed at lower latitudes and the separation between these zones is not as distinct as it is in the distribution from the S15 model with simple geography. Other common characteristics among the distributions of changes obtained from the three models include an increase of zonal mean soil moisture in high latitudes during the period from fall to spring. Although it is possible that the changes in zonal mean soil moisture described above are essentially a manifestation of sampling error, the similarly among the results from the three models strongly suggest that they are caused by the increase of CO_2-concentration in the model atmosphere.

In the subtropics and tropics, the pattern of change in zonal mean soil moisture varies among the results from the three models. Thus, it is not possible to identify common characteristics in the distributions of soil moisture change in these latitudes. Since the precipitation in low latitudes of the model is highly sporadic, it is necessary to average the value of soil moisture over a very extended period of time in order to distinguish the CO_2-induced change from the natural fluctuation of soil moisture of the model.

To evaluate the statistical significance of the difference in zonal mean soil moisture between the two experiments with the S15 model, the 'Student' t test is conducted as suggested by Chervin and Schneider (1976). In the Student t test, the t-value is computed from the following formula.

$$t = \Delta[w]/\sigma_\Delta \tag{1}$$

where $\Delta[w]$ is the difference in time averaged zonal mean soil moisture between the 4 x CO_2- and the standard experiments and σ_Δ is the standard deviation of the difference $\Delta[w]$. Based upon the assumption that the values of soil moisture from each year are independent and have nearly a normal distribution, the standard deviation σ_Δ may be computed by the following equation (Panofsky and Brier, 1965)

$$\sigma_\Delta = \sqrt{\frac{(N_1 - 1)\,\sigma_1^{\,2} + (N_2 - 1)\,\sigma_2^{\,2}}{N_1 + N_2 - 2} \cdot \left(\frac{1}{N_1} + \frac{1}{N_2}\right)} \tag{2}$$

where N_1 and N_2 are the numbers of the time mean, zonal mean soil moisture samples from the 4 x CO_2- and the standard experiments, respectively. σ_1 and σ_2 are standard deviations of these soil moisture values from the two experiments. Since 8 samples are available from each experiment, $N_1 = N_2 = 8$ for the present situation. To facilitate the identification of the zones where the difference is statiscally significant, the t-values are normalized (i.e., divided) by $t_{n,\alpha/2}$, and are shown in Figure 9. Here, $t_{n,\alpha/2}$ is the critical value of t which is determined such that it satisfies the following relationship.

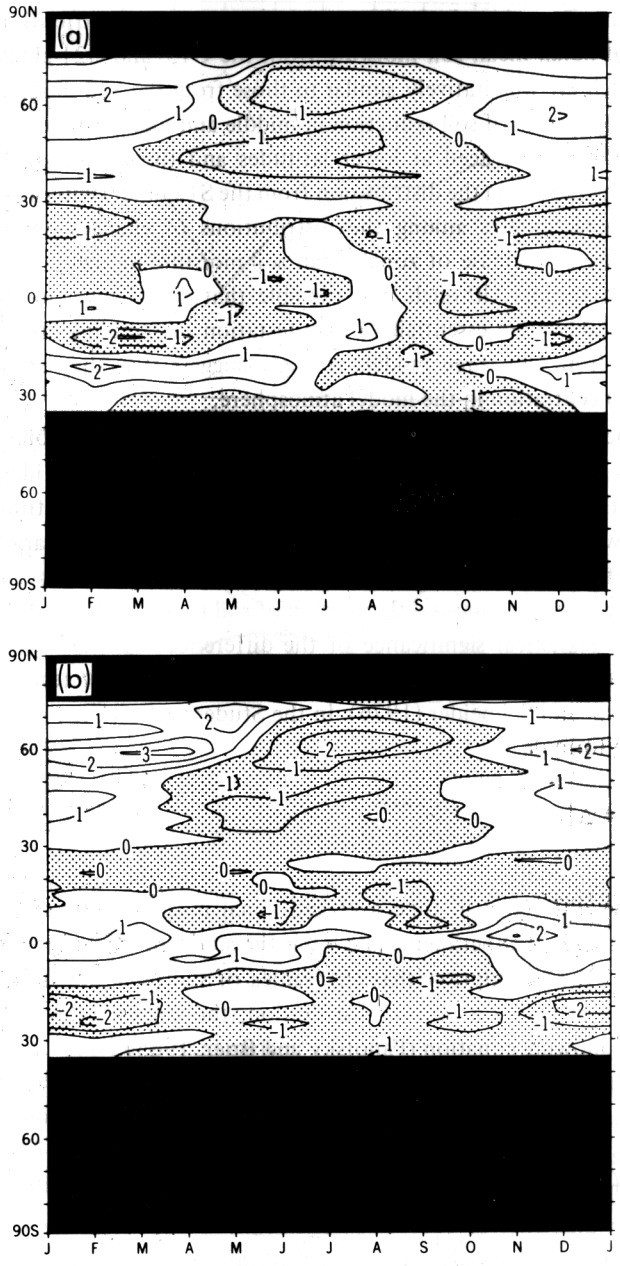

Fig. 8. The latitudinal and seasonal variation of zonal mean soil moisture difference (cm) between the 4 x CO_2- and the standard experiments for (a) the G15 model (same as Figure 27 of Manabe and Stouffer, 1980), and (b) the G21 model. The distribution is not shown in high latitudes of both hemispheres or middle latitudes of the Southern Hemisphere, because most of these zones are occupied by either continental ice sheets or oceans.

$$\text{Prob.}\{|t| \geq t_{n,\alpha/2}\} = \alpha$$

where Prob.{ } indicates the probability that the condition indicated in the brackets is satisfied and α is the confidence criterion. (Given the degree of freedom, $n = N_1 + N_2 - 2$ (= 8 + 8 − 2 = 14) and α = 0.1, the critical t-value is 1.76 from Table 14 of Panofsky and Brier, 1968). If the normalized t-value shown in Figure 9 is greater than unity, the null hypothesis that the difference in zonal mean soil moisture is zero (i.e., $\Delta[w] = 0$) can be rejected at the 90% confidence level.

According to Figure 9, the negative differences of zonal mean soil moisture in the two zones of middle and high latitudes during summer are statistically significant at the 90% (or higher) confidence level. This figure also indicates that the positive difference of zonal mean soil moisture in high latitude appearing from fall to spring is particularly significant. On the other hand, the difference of soil moisture in low latitudes is less significant even though the percentage difference is very large as indicated by Figure 7c. As pointed out already, a very long term averaging of soil moisture is required before one can obtain statistically significant results in these latitudes.

To illustrate the uncertainty involved in the estimate of the soil moisture difference $\Delta[w]$, one can define the confidence interval, d, of $\Delta[w]$ by the following equation as suggested by Hayashi (1982).

$$d = t_{n,\alpha/2} \times \sigma_{\Delta}. \tag{3}$$

Here, d is chosen such that the probability that the true value of zonal mean soil moisture difference lies between $\Delta[w]+d$ and $\Delta[w]-d$ is $(1-\alpha)$. From the Equations (1) and (3),

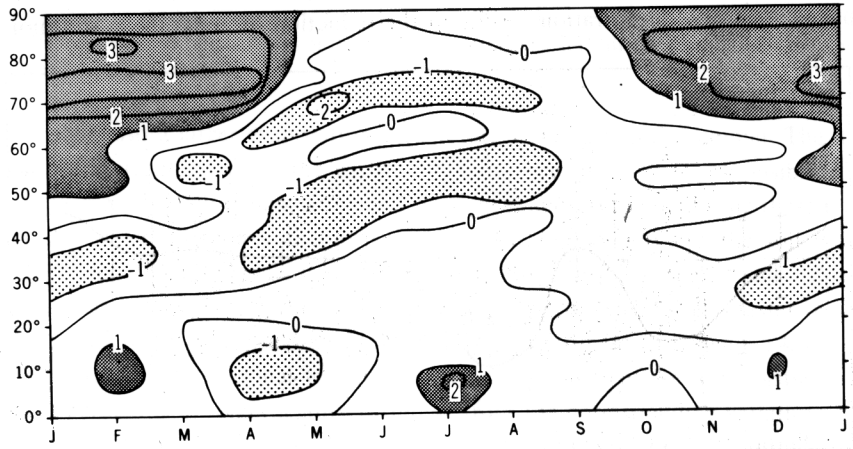

Fig. 9. The latitudinal and seasonal variation of the normalized Students t values for the difference in zonal mean soil moisture between the 4 x CO_2- and the standard experiments with the S15 model. Here, t value is normalized by the critical t value for the confidence level of 90%. See the main text for further details. The distribution of the two hemispheres of the model are averaged after shifting the phase of the southern hemisphere-variation by six months.

one can derive the following equation relating the normalized t-value defined above and confidence interval.

$$t/t_{n,\alpha/2} = \Delta[w]/d.$$

In Figure 10, which shows that latitudinal distribution of the difference in zonal mean soil moisture averaged over the three summer months, 90% confidence intervals are indicated by vertical line segments. Again, this figure clearly illustrates the statistical significance of the summer-reduction of zonal mean soil moisture in middle and high latitudes described in the preceding paragraph. On the other hand, the difference in zonal mean soil moisture is not statistically significant in low latitudes. In the arid zone of 30° ∿ 40° latitude, the difference is significantly small. For a further statistical assessment of the present result, see Hayashi (1982).

To illustrate the variability characteristics of the difference in zonal mean soil moisture between the 4 x CO_2- and the standard experiments, Figure 11 is constructed. A distribution of the zonal mean difference averaged over three summer months is computed from each of the four years chosen for the present analysis. To avoid congestion of lines, the distrbutions for the Northern and Southern Hemisphere are shown separately. Although there are large differences among the profiles shown in this figure, six out of eight distributions indicate two instinct zonal belts of negative difference in middle and high latitudes suggesting that the double belt of relatively large negative difference tends to occur and is indeed CO_2-induced. On the other hand, the sign of zonal mean soil moisture difference in low latitudes varies from one sample distribution to another indicating that the difference is not statistically significant.

The results from the Student t test described above support the inference derived earlier from the intercomparison of the results from three different models: the increase of atmospheric CO_2-concentration results in the reduction of zonal mean soil moisture

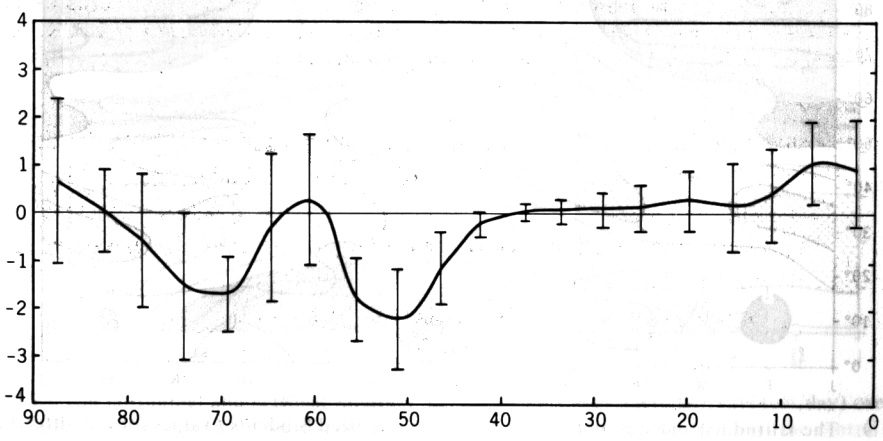

Fig. 10. Latitudinal distribution of the difference in zonal mean soil moisture averaged over the three months (i.e., June, July and August) for the S15 model. Vertical line segments indicate 90% confidence intervals. Units are in cm.

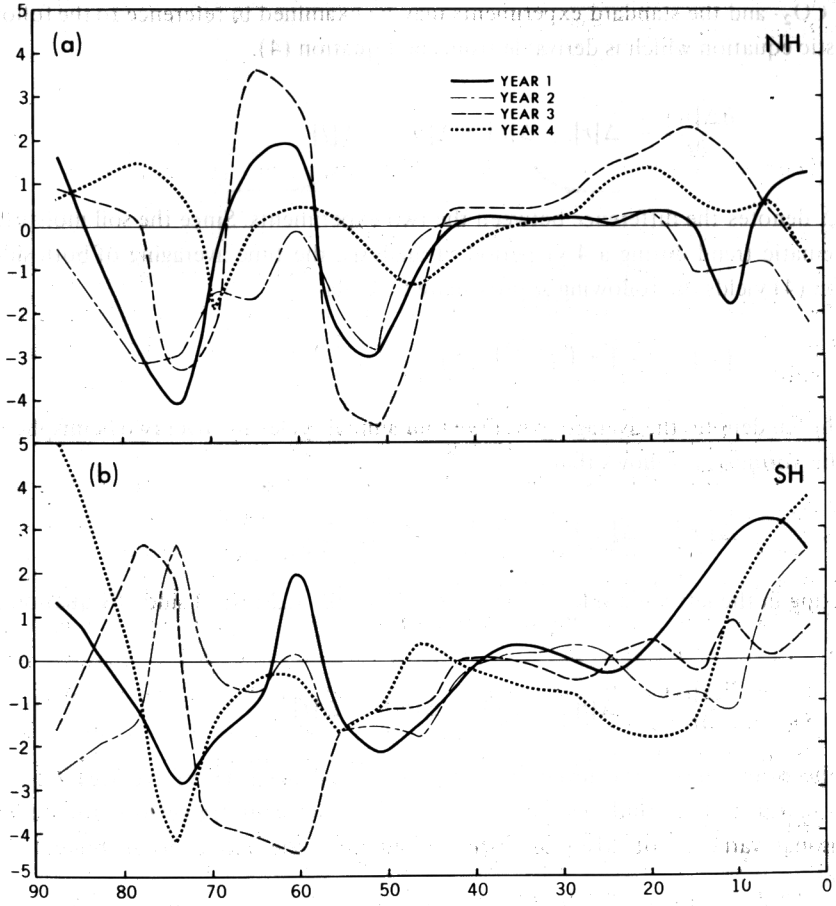

Fig. 11. Latitudinal distribution of the CO_2-induced difference in zonal mean soil moisture averaged over the three summer months for each of the four years of the S15 model analysis period. Results are for (a) the northern hemisphere and (b) the southern hemisphere. Units are in cm.

in middle and high latitudes during summer. To identify the mechanism for the CO_2-induced summer dryness, the seasonal variation of soil moisture budget from both 4 x CO_2- and standard experiments with various models is examined. Before getting into the detailed discussion of the results, it is convenient to briefly describe the relevant equations describing the budget of soil moisture.

The prognostic equation of soil moisture may be written as

$$\frac{\partial [w]}{\partial t} = [r] - [e] + [m] - [f] \tag{4}$$

where w is soil moisture, r is the rate of rainfall, e is the rate of evaporation, m is the rate of snowmelt, f is the rate of runoff and [ ] denotes a zonal average over continents.

The seasonal variation of the difference in the zonal mean soil moisture budget between

the 4 x CO_2- and the standard experiments may be examined in reference to the following prognostic equation which is derivable from the Equation (4).

$$\frac{\partial \Delta[w]}{\partial t} = \Delta[r] - \Delta[e] + \Delta[m] - \Delta[f] \tag{5}$$

where Δ denotes the difference between the two experiments. Since the soil moisture has no systematic trend during a 4 yr period of analysis, the time averaging of both sides of Equation (4) yields the following approximate formula

$$[\bar{r}] - [\bar{e}] + [\bar{m}] - [\bar{f}] \simeq 0 \tag{6}$$

where the bar denotes the averaging over the four annual cycles and over two hemispheres. From this formula, it follows that

$$\Delta[\bar{r}] - \Delta[\bar{e}] + \Delta[\bar{m}] - \Delta[\bar{f}] \simeq 0 . \tag{7}$$

Subtracting in the left hand side of formula (7) from the right hand side of Equation (5), one gets

$$\frac{\partial \Delta[w]}{\partial t} \simeq \Delta[r]' - \Delta[e]' + \Delta[m]' - \Delta[f]' \tag{8}$$

where the prime denotes a deviation from the annual mean (8 yr average). Compared with Equation (5), formula (8) provides a more convenient framework for discussing the seasonal variation of $\Delta[w]$ as distinguished from the annual mean budget of soil moisture.

Some of the results from the analysis of soil moisture budget of the S15 model are shown in Figures 12 and 13. For example, Figure 12a, b, 13a and b illustrate the seasonal variation of $[r]$, $-[e]$, $[m]$, and $-[f]$ from the 4 x CO_2- and the standard experiments for two selected latitudes of 72 and 52° where the CO_2-induced summer dryness is most pronounced. The difference of these components between the two experiments (i.e. $\Delta[r]$, $-\Delta[e]$, $\Delta[m]$, and $-\Delta[f]$) are shown in Figures 12c and 13c. An annual mean value of each difference is indicated on the right hand side of these figures so that one can determine $\Delta[r]'$, $-\Delta[e]'$, $\Delta[m]'$, and $-\Delta[f]'$ by visually subtracting the annual mean from the original values whenever it is necessary. (See Appendix I for the description of the distribution of the annual mean budget of soil moisture.) In addition, the seasonal variations of zonal mean soil moisture obtained from the two experiments are shown in Figures 14a and b for both 72 and 52° latitude.

From the inspection of Figure 14a, one notes that, in both experiments, the zonal mean soil moisture is near saturation (i.e., 15 cm) at 72° latitude in late spring when the rate of snowmelt is at a maximum. It gradually reduces from the peak value in late spring to the lowest values in summer. A comparison between Figures 12a and b indicates that the rate of snowmelt in the 4 x CO_2- experiment attains its maximum value earlier by

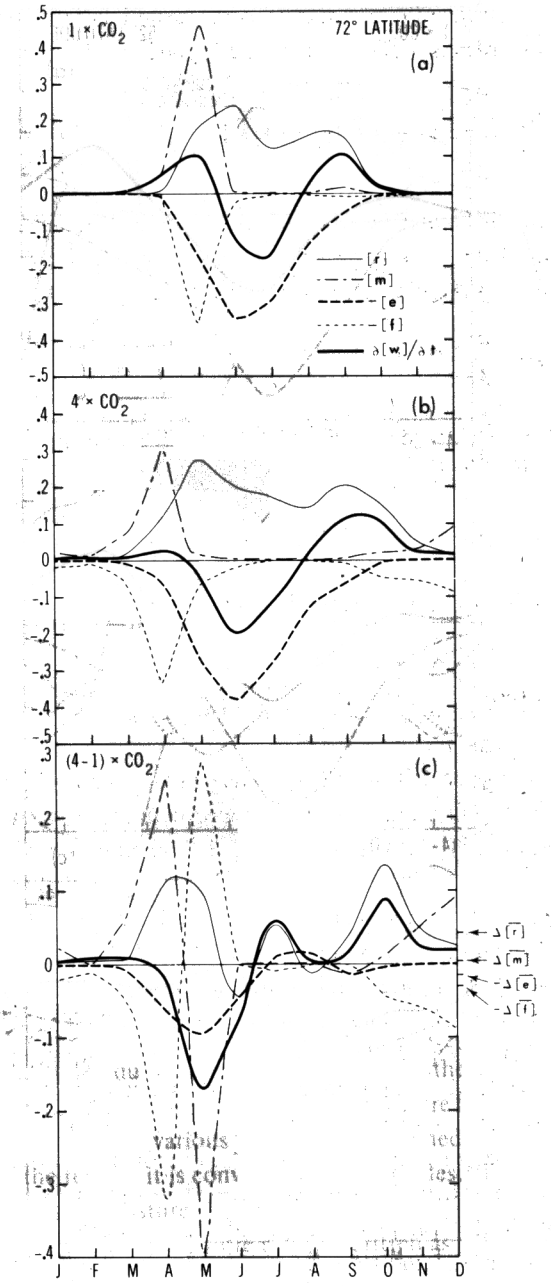

Fig. 12. Seasonal variation of the various components of the S15 model soil moisture budget (cm/day) at the 72° latitude circle for (a) the standard experiment, (b) the 4 x CO_2-experiment and (c) the difference between the 4 x CO_2- and the standard experiments. (In addition, the annual mean differences of these components are indicated on the right hand side of the figure). Here r is the rate of rainfall, m is the rate of snowmelt, e is the rate of evaporation and f is the rate of runoff. The net rate of change of soil moisture is denoted by $\partial[w]/\partial t$. See the main text for further explanation. The individual components are denoted by various types of thin lines, whereas the net change is indicated by a solid, heavy line. The results from the two hemispheres are averaged after shifting the phase of the Southern Hemisphere variation by six months.

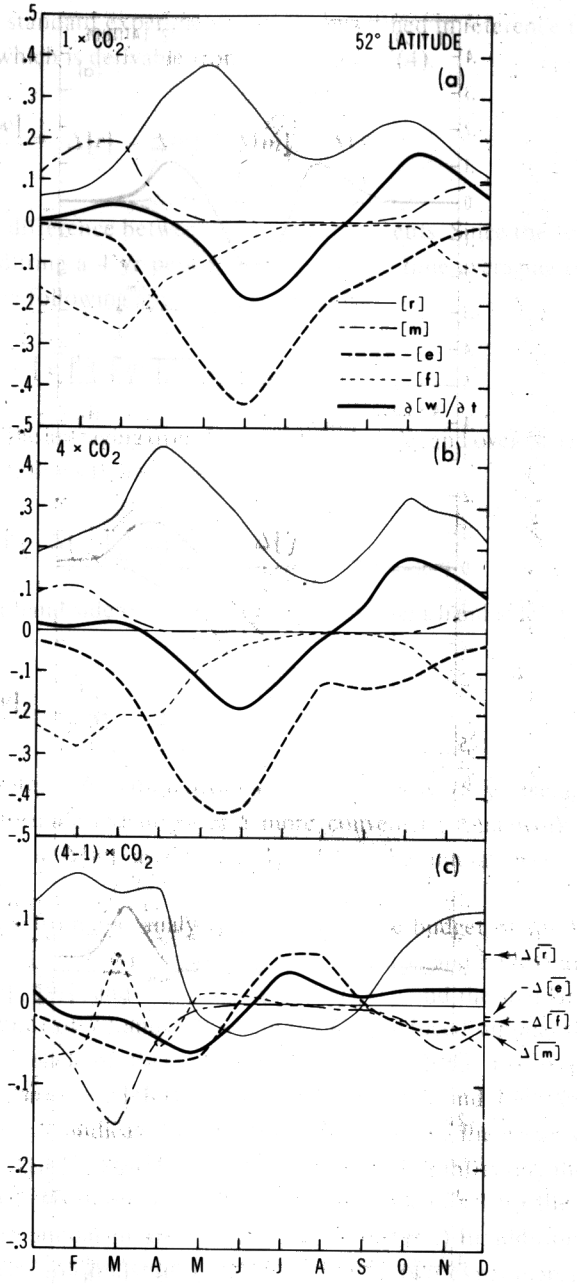

Fig. 13. Same as Figure 12 except at the 52° latitude circle.

about one month as compared with the standard experiment. Thus, in the 4 x CO_2-experiment the spring to summer reduction of soil moisture begins earlier, resulting in the smaller value of soil moisture in summer. It is important to recognize that, in the 4 x CO_2-experiment, the earlier timing of the snowmelt season results in not only a smaller rate of

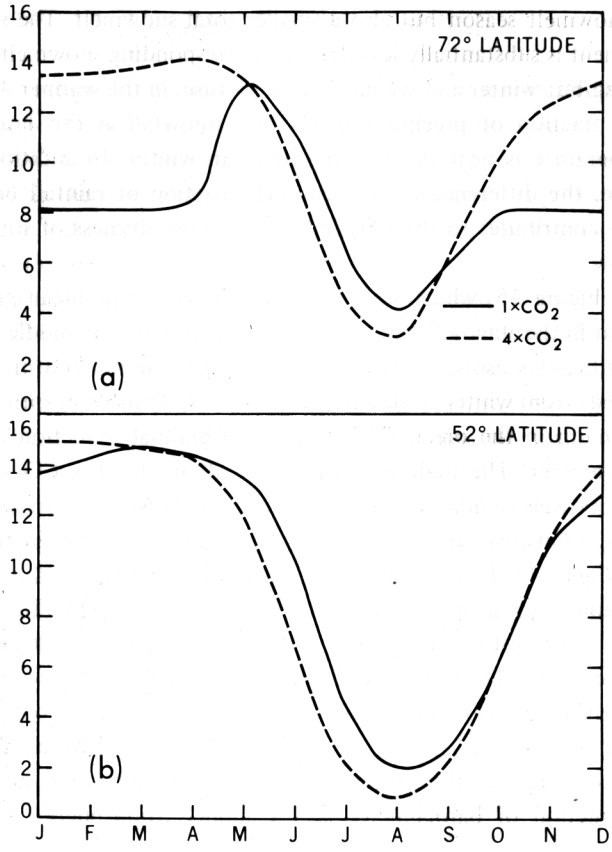

Fig. 14. Seasonal variation of zonal mean soil moisture (cm) at (a) the 72° latitude, and (b) the 52° latitude of the S15 model. The results from both 4 x CO_2- and the standard experiments are shown. The results from the two hemispheres of the model are averaged after shifting the phase of the Southern Hemisphere by six months.

snowmelt but also a larger evaporation rate in late spring and early summer. The smaller surface albedo resulting from the earlier disappearance of snow is responsible for the larger surface absorption of insolation and stronger evaporation rate during these seasons. Figure 12c, which illustrates the difference in the components of the soil moisture budget between two experiments, clearly shows that $\Delta[m]$ (or $\Delta[m]'$) and $-\Delta[e]$ (or $-\Delta[e]'$) are negative in late spring and early summer accounting for the faster reduction of soil moisture during these seasons in the 4 x CO_2-experiment (see Figure 14a).

At 52° latitude, the seasonal variations of the components of the soil moisture budget in both experiments are significantly different from the corresponding variations at 72° latitude discussed above. For example, the relative magnitude of the contribution of snowmelt to the soil moisture budget at this latitude is somewhat smaller than the contribution at 72° latitude. Nevertheless, the smaller rate of snowmelt and stronger evaporation accounts for the faster reduction of soil moisture during the late spring and early summer in the 4 x CO_2-experiment. This smaller snowmelt in spring results not only from the earlier

timing of the snowmelt season but also a smaller total snowmelt. The snowmelt in the 4 x CO_2-experiment is substantially less than the corresponding snowmelt in the standard experiment during but winter and spring. This is because, in the warmer 4 x CO_2-climate, a much smaller fraction of precipitation becomes snowfall at this latitude where the surface air temperature is near the freezing point in winter. In addition to the effects considered above, the difference in the seasonal variation of rainfall between the two experiments also contributes to the CO_2-induced summer dryness of soil at this latitude as discussed below.

According to Figure 15, which shows the variation of zonal mean precipitation rate over the continent in the standard experiment, the location of the middle latitude rainbelt undergoes a significant seasonal variation. For example, the rainbelt moves poleward as the season proceeds from winter to summer. It passes 52° latitude in spring accounting for the spring maximum in the precipation rate and a gradual reduction of soil moisture from spring to summer. The middle latitude rainbelt in the 4 x CO_2-experiment also undergoes a qualitatively similar seasonal excursion. It, however, is located polewards of the corresponding rainbelt in the standard experiment by several degrees as indicated by a dashed line in Figure 15. This accounts for the earlier occurrence of the spring maximum in the precipitation rate, the earlier beginning of soil moisture reduction from spring to summer and less soil moisture in summer in the 4 x CO_2-experiment as compared with the standard experiment. The CO_2-induced shift of the middle latitude rainbelt described above is due partly to the penetration of warm, moisture rich air into high latitudes. For further discussion of this topic, refer to the study of Manabe and Wetherald (1980).

The earlier occurrence of the spring maximum in rainfall rate is also caused by the CO_2-induced reduction of baroclinicity in the model troposphere. According to the

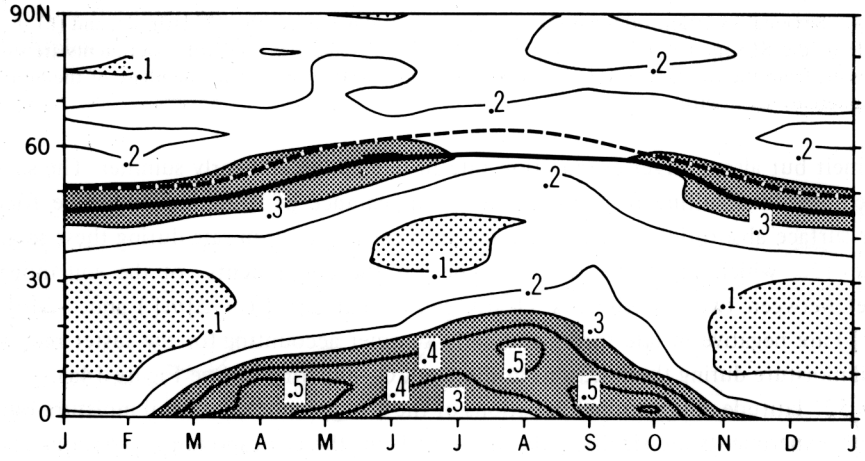

Fig. 15. The latitudinal and seasonal variation of the zonal mean precipitation rate (cm/day) over the continent from the standard experiment with the S15 model. The solid line indicates the central position of the middle latitude rainbelt for the standard experiment, whereas the dashed line represents the central position of the corresponding middle latitude rainbelt for the 4 x CO_2-experiment. The distributions of the two hemispheres of the model are averaged after shifting the phase of the southern hemisphere variation by six months.

comparison of the results from the 4 x CO_2- and the standard experiments, the meridional temperature gradient reduces and the summer period of weak baroclinicity (i.e., smaller eddy kinetic energy in the model troposphere) becomes longer. (See Figure A5 of Appendix II for an illustration of the difference in eddy kinetic energy between the two experiments.) Because of the change in eddy kinetic energy described above, the rainfall maximum occurs earlier in spring and later in the fall in middle and high latitudes as the comparison between Figures 13a and b indicates.

From an inspection of Figure 13c, which includes an illustration of the seasonal variation of the difference in rainfall rate between the two experiments at 52° N, it is clear that the difference in total rainfall over an entire year is positive, indicating the CO_2-induced increase of annual rainfall at this latitude (see Appendix I). One notes, however, that the difference in rainfall rate (i.e., $\Delta[r]$) undergoes a large seasonal variation. It decreases rapidly from the peak positive value in spring to negative values in summer resulting from the earlier occurrence of the spring rainfall maximum in the 4 x CO_2-experiment discussed above. Thus, $\Delta[r]'$ also undergoes a qualitatively similar variation and makes $\partial\Delta[w]/\partial t$ negative in late spring and early summer.

In short, the CO_2-induced dryness of soil in summer results not only from the earlier ending of the snowmelt season, but also from the earlier occurrence of the spring to summer-reduction in rainfall rate. The former effect is particularly important in high latitudes, whereas the latter effect becomes important in middle latitudes.

To examine the mechanisms for the CO_2-induced changes in soil moisture of the global models, the seasonal variation of differences in various components of the zonal mean soil moisture budget between the 4 x CO_2- and the standard experiments are computed. Since the results from the G15 and G21 models are essentially similar to one another, these two sets of results are averaged with one another to reduce the sampling error. Figures 16a and b illustrate the annual marches of the differences in various soil moisture budget components at two selected latitudes, i.e., 60N and 45N where the CO_2-induced reduction of soil moisture during summer is most pronounced. For reference, the seasonal variations of zonal mean soil moisture from both experiments at these two latitudes are shown in Figure 17.

According to Figure 16a, the seasonal variation of the differences in the soil moisture budget at 60° N of the global models is qualitatively similar to the corresponding variation at 72° latitude of the S15 model discussed earlier. However, the temporal variation of the rates of snowmelt and runoff in spring is much more gradual than the corresponding change from the S15 model. This is because the timing of the snowmelt season from the global models has a larger longitudinal variation due to the topographic influences.

Figure 16a indicates that $\Delta[m]$ and $\Delta[m]'$ are negative in late spring and early summer because of the earlier ending of the snowmelt season in the 4 x CO_2-experiment as compared with the standard experiment. In addition, $-\Delta[e]$ and $-\Delta[e]'$ are negative in late spring. Thus, $\partial\Delta[w]/\partial t$ becomes negative in late spring implying the development of the CO_2-induced summer dryness. This is also evident in Figure 17a, which shows that $\Delta[w]$ is positive in spring but is negative in summer. The seasonal variation of the soil moisture budget of the global models described above is qualitatively similar to the corresponding

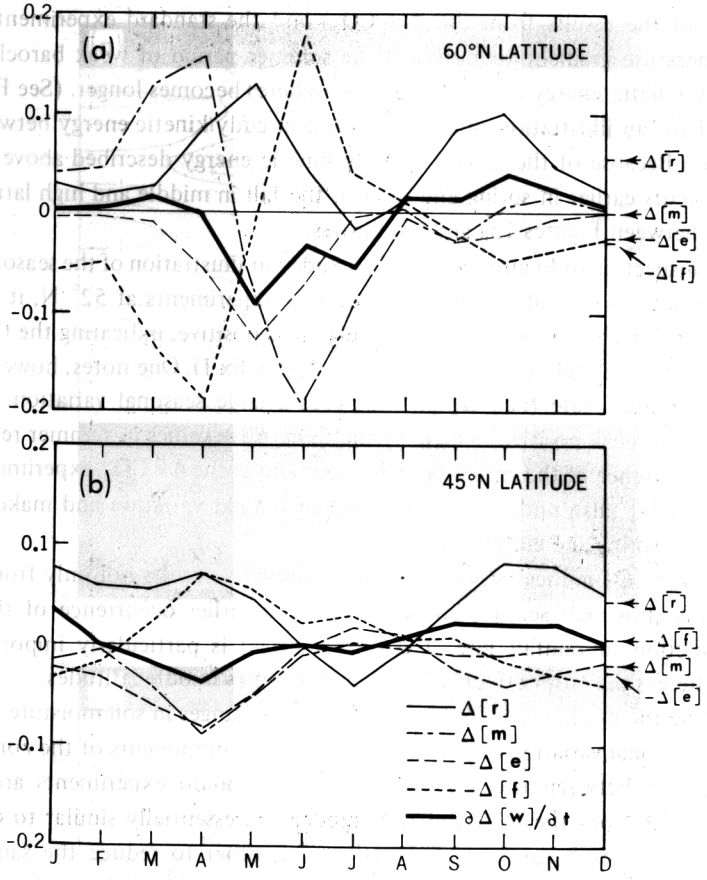

Fig. 16. Seasonal variation of the zonal mean difference in various components of soil moisture budget between 4 x CO_2- and the standard experiments. The results from the G15 and G21 models are averaged together. Units are in cm/day. The distributions at (a) 60° N and (b) 45° N are shown here. For the definitions of notations, see the main text or the caption of Figure 12.

variation of the S15 model discussed earlier.

At 45° N of the global models, Figure 16b, both $\Delta[m]'$ and $-\Delta[e]'$ are negative in spring and are responsible for making $\partial\Delta[w]/\partial t$ negative in that season as they are at 52° latitude of the S15 model. Figure 16b also indicated that $\Delta[r]$ reduces from spring to summer in qualitative agreement with the behavior of the S15 model. The temporal reduction of $\Delta[r]$ is, however, more gradual than the corresponding reduction in the results of the S15 model, because the middle latitude-maximum in zonal mean rainfall rate of the global models with orography is defined less sharply than that of the S15 model with a flat land surface.

One can evaluate how the difference in rainfall rate contributes to the CO_2-induced summer dryness by reexamining Figure 16b in the light of the prognostic formula (8), which distinguishes the seasonal budget from the annual budget of soil moisture. According to this figure, $\Delta[r]'$ is positive in spring but is negative during the summer

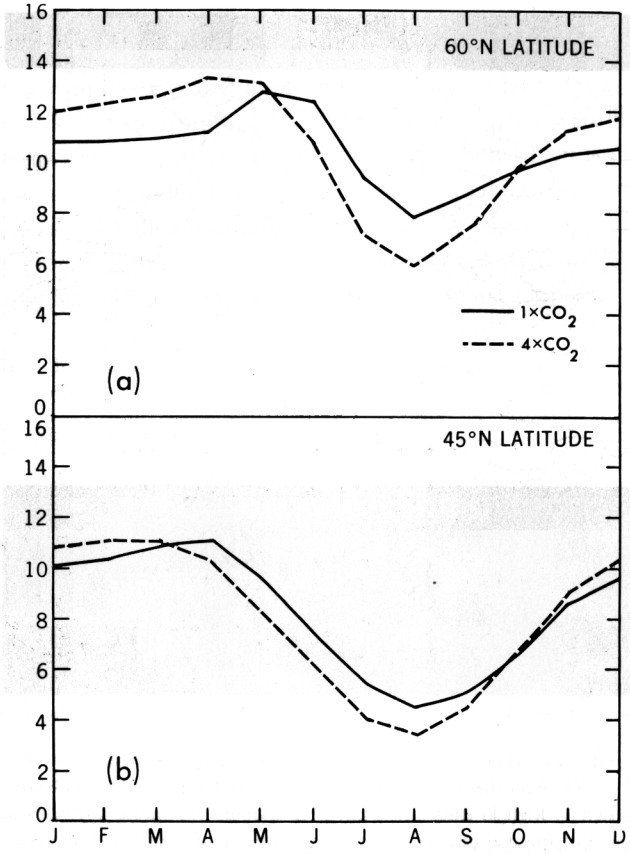

Fig. 17. Seasonal variation of zonal mean soil moisture (cm) from the global models with realistic geography for the 4 x CO_2- and the standard experiments, separately. Results from both the G15 and G21 models are averaged together and are shown for the latitudes of (a) 60° N, and (b) 45° N.

season. Because of the negative contribution of $\Delta[r]'$, $\Delta[w]$ remains negative in summer despite the positive contributions of $\Delta[m]'$ and $-\Delta[e]'$.

In short, the earlier ending of the snowmelt season followed by the period of more intense evaporation accounts for the development of the CO_2-induced summer dryness in middle latitudes. In addition, the earlier beginning of the spring to summer reduction of rainfall rate helps maintain the CO_2-induced dryness during most of the summer.

Figure 18 indicates that the percentage of the CO_2-induced reduction of zonal mean soil moisture in summer ranges from 10 $\sim$ 25% of the original value at 45° N of the global models. This percentage change is somewhat smaller than the corrsponding change in zonal mean soil moisture in middle latitudes of the sector model (see Figures 7c and 14b). This is consistent with the fact that, in the global model with realistic geography, the distribution of the CO_2-induced soil moisture change is less zonal than the corresponding distribution for the sector model.

As pointed out already the two zones of reduced soil wetness in the global models are located at lower latitudes than the corresponding zones in the S15 model with idealized

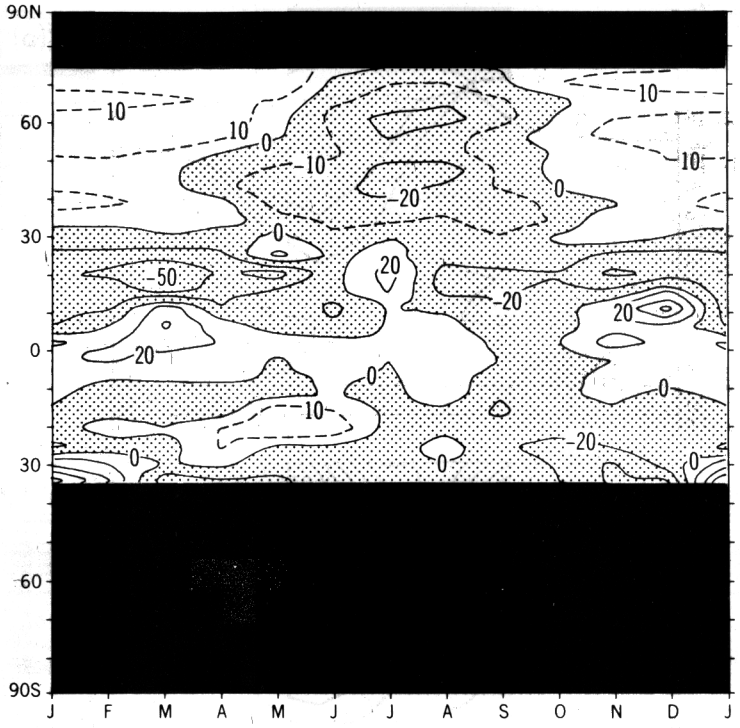

Fig. 18. Latitudinal and seasonal variation of the percentage change of zonal mean soil moisture from the standard to the 4 x CO_2-experiments (the results from the two global models are averaged). The distribution is not shown in high latitudes of both hemispheres or middle latitudes of the Southern Hemisphere because most of these zones are occupied by either continental ice sheets or oceans.

geography. The surface air temperature in high latitudes of the S15 model is significantly higher than the global models (Wetherald and Manabe, 1981) resulting in the poleward shift of the pattern of the CO_2-induced hydrologic change. Since the zonal mean surface air temperature in high latitudes (the Northern Hemisphere) of the global models is more realistic than the corresponding temperature of the S15 model, it is reasonable to place more confidence on the results from the global models with respect to the latitudinal placement of the zones of maximum soil moisture reduction.

It was previously shown that the area of increased aridity during summer in high latitudes is caused by the earlier melting of the continental snow pack and, therefore, a lenghtening of the drying season. The earlier timing of the snowmelt season also manifests itself in the latitude-time distribution of the difference in the runoff rate between the 4 x CO_2- and standard experiments for the G21 model (Figure 19). Polewards of 50N, there are two parallel bands of significant differences, one positive and the other negative during the spring season. These two parallel bands of runoff differences indicate the earlier occurrence of the spring maximum in runoff rate in the 4 x CO_2-experiment as compared with the standard experiment. (As one can infer from Figure 29 of the paper by Manabe and Stouffer, the difference in timing is approximately 1 ~ 2 months depending upon latitude.) In middle latitudes, a zone of smaller negative difference is apparent during

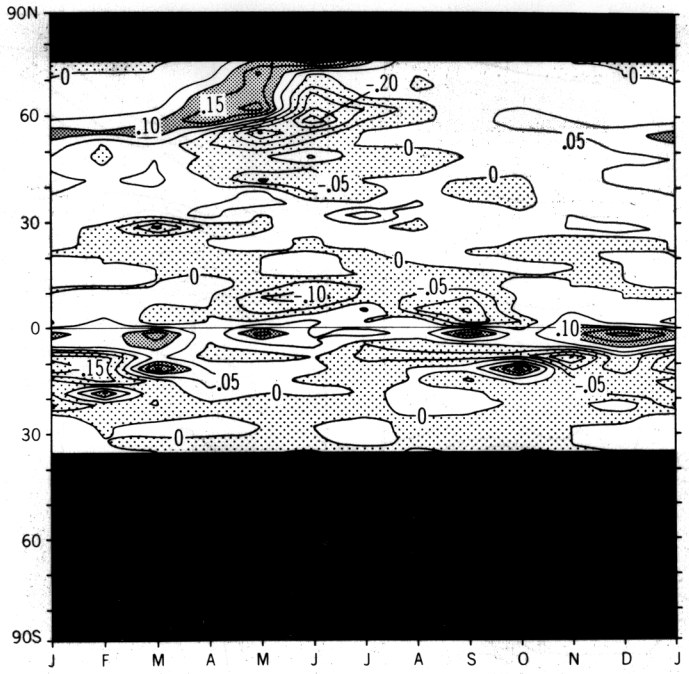

Fig. 19. The latitudinal and seasonal variation of the difference in zonal mean runoff rate (cm/day) between the 4 x CO_2- and the standard experiments for the G21 model. The distribution is not shown in high latitudes of both hemispheres or middle latitudes of the Southern Hemisphere because most of these zones are occupied by either continental ice sheets or oceans.

late spring and early summer and is a consequence of the earlier occurrence of the spring to summer reduction of rainfall rate in the 4 x CO_2-experiment discussed earlier. Since the soil moisture is substantially below saturation during the summer months for both middle and high latitudes (see Figure 6a), there is very little change in the runoff rate for the remainder of the summer season.

4.2. Geographical distribution

This subsection deals with the geographical change of soil moisture caused by the quadrupling of CO_2. As has been done previously, the discussion begins with the S15 model and then proceeds to the G15 and G21 models. Figures 20a and b show the differences of soil moisture obtained from the S15 model for the spring and summer seasons respectively. In particular, Figure 20a indicates an almost zonal belt of soil moisture reduction centered approximately at 45° latitude for the spring season and a region of increased wetness in higher latitudes. For the summer distribution, there are two separate zones of increased dryness; one centered at middle latitudes and the other at high latitudes (Figure 20b). These features are consistent with the time-latitude difference distribution shown earlier for the S15 model (Figure 7a).

These two zones of increased dryness during summer also have a significant impact on

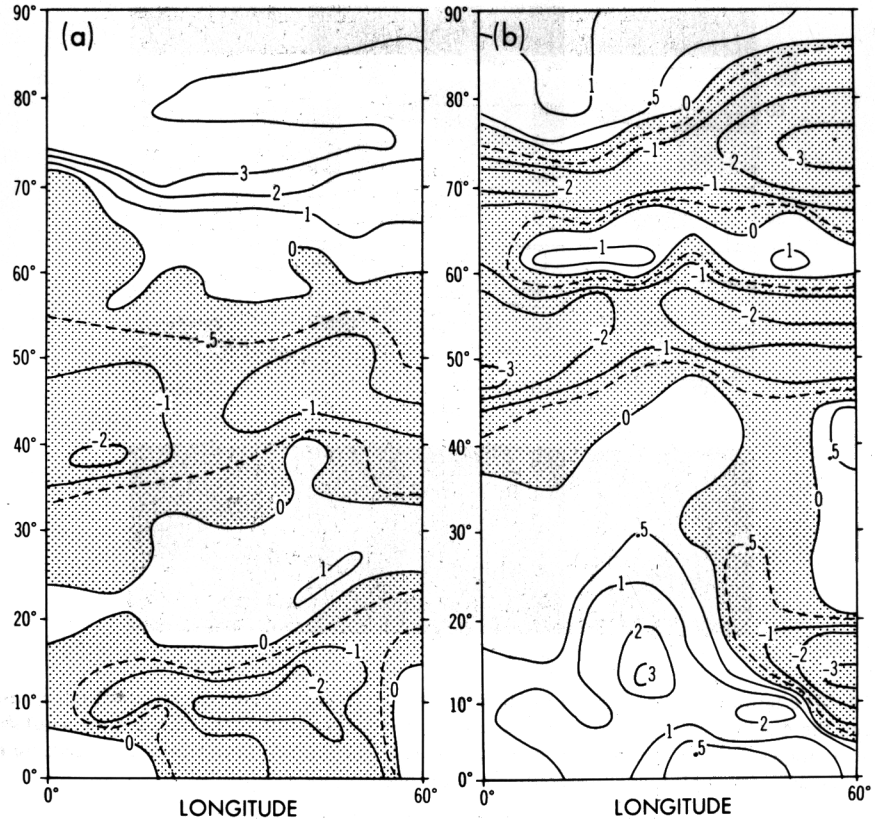

Fig. 20. Geographical distribution (over the continent) of the difference of the S15 model soil moisture (cm) between the 4 x CO_2- and the standard experiments for the (a) spring season, and (b) summer season. The distribution of the two hemispheres of the model are averaged after shifting the phase of the southern hemisphere variation by six months.

the change of surface air temperature shown in Figure 21. As this figure indicates, there are two zones of maximum surface air temperature increase which correspond to the position of the two zones of increased aridity. In these zones, the surface heat loss by evaporation is suppressed and contributes to the warming of the surface temperature. A similar mechanism was evident in the study by Manabe and Wetherald (1980). The temperature increase in the high latitude dry zone is not as great as the corresponding increase in the middle latitude zone because of the following reasons: (1) the percentage reduction of soil moisture is not as great at high latitudes as it is for middle latitudes (see Figure 7c); (2) in summer, the CO_2-induced warming of surface air over the high latitude portion of a continent is constrained by the influence of the polar ocean which has a small CO_2-induced surface warming in this season. (See Manabe and Stouffer (1980) for a discussion of the mechanism responsible for the small summer warming in high latitudes.)

The situation is more complicated in the case of the global general circulation models (G15, G21). Figure 22a and b show the geographical distribution of soil moisture difference

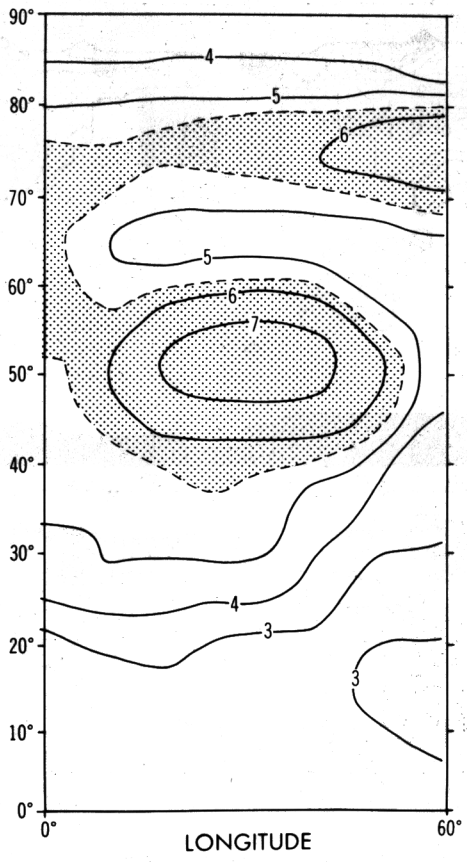

Fig. 21. Geographical distribution (over the continent) of the difference of the S15 model surface air temperature (°C) between the 4 x CO_2- and the standard experiments for the summer season. The distribution of the two hemispheres of the model are averaged after shifting the phase of the southern hemisphere variation by six months.

obtained from the G15 and G21 models, respectively, for the spring (March-April-May) season. (Small scale features have been removed from these figures by the application of 2-dimensional binomial filters.) Qualitatively, the same general pattern exists for both model distributions in the Northern Hemisphere. For example, there is a general increase of wetness in high latitudes and a reduction of wetness in middle latitudes over both the Asian and North American continents although the local details of these changes of wetness differ significantly from one model to the other. Similar large scale features are present for the spring distribution of soil moisture differences as obtained from the S15 model (Figure 20a). Areas of local differences between the G15 and G21 models include the extreme southeastern United States, southeastern and northeastern Asia, and South America.

The corresponding summer distributions for both the G15 and G21 models are shown in Figures 23a and b, respectively. Here, both models indicate the same qualitative pattern of soil moisture changes although, again, local differences exist. For example,

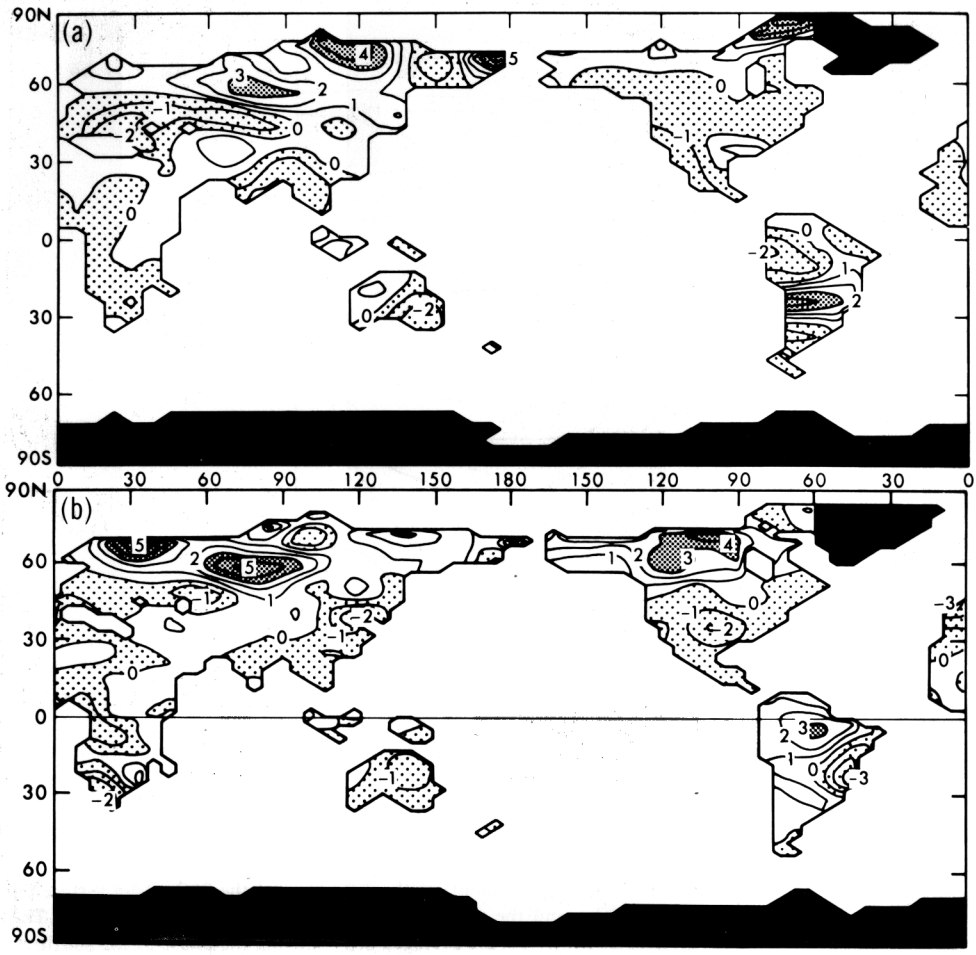

Fig. 22. Geographical distribution of the difference of soil moisture (cm) between the 4 x CO_2- and the standard experiments obtained for the (March-April-May) period. (a) the G15 model, (b) the G21 model. Here, 2-dimensional binomial filters are applied to the results to eliminate scales smaller than 2 grid lengths which are approximately 9° latitude.

both models show a general reduction of soil moisture over both middle and high latitudes for Asia and North America. This large latitudinal area of reduced wetness is qualitatively similar to the corresponding distribution obtained from the S15 model (Figure 20b) although the distinction between the two separate zones of increased aridity identified previously is not as evident for the G21 model as it is for both S15 and G15 models. In particular, the soil moisture does not reduce significantly over the United States for the G21 model as it does for the G15 model. This is due to the fact that the soil is very dry in the southwestern United States at the beginning of the summer season in the G21 model standard simulation (see Section 3) and, therefore, it is not possible to reduce the soil moisture there much further. Although there are some other local differences between the two models such as over southeastern Asia, equatorial Africa, and South America,

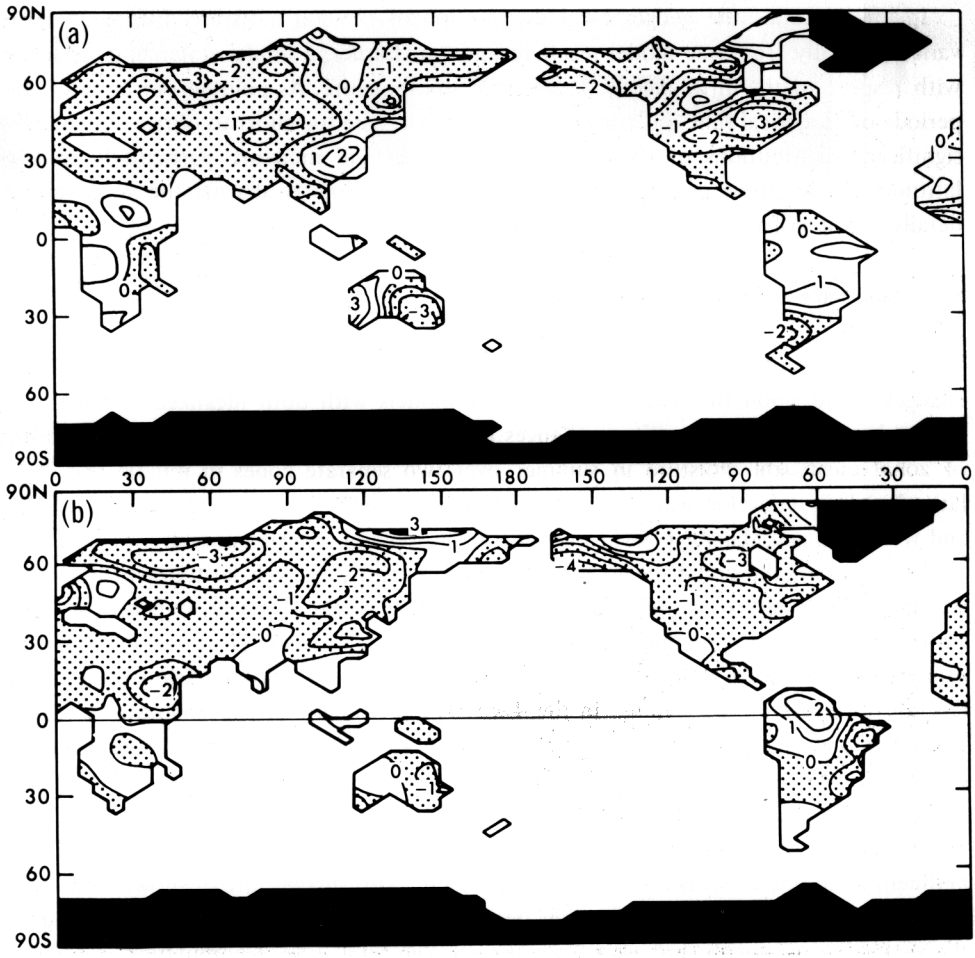

Fig. 23. Geographical distribution of the difference of soil moisture (cm) between the 4 x CO_2- and the standard experiments obtained for the (June-July-August) period, (a) the G15 model. (b) the G21 model. A spatial filter is applied to the results as described in the caption of Figure 22.

the general observation of a summer soil moisture reduction appears to hold true for both global model experiments. These results, taken together with the statistical analysis performed on the S15 model, suggest that this overall increase of aridity during the summer season in middle and high latitudes is a common and significant feature of all the experiments considered in this study. However, it is difficult to determine the details in the geographical distribution of the CO_2-induced soil moisture change in these latitudes because this aspect of the results suffers from large sampling errors, is highly model-dependent, and thus varies from one set of experiments to another.

It should be mentioned that, in summer, a correspondence exists between areas of increased temperature and regions of soil moisture reduction similar to that identified for the S15 model. This may be seen by comparing Figure 23a of the present paper with Figure 23c of the paper by Manabe and Stouffer (1980).

In low latitudes, the geographical distribution of the soil moisture difference again varies markedly from one model result to another. Earlier, a similar statement was made with respect to the difference in zonal mean soil moisture. As pointed out already, the periods of numerical time integrations of these models are too short to obtain statistically significant distributions of CO_2-induced changes in soil moisture particularly in low latitudes. Under these circumstances, it is not worth-while to discuss the geographical details of soil moisture differences in these latitudes.

5. Summary and Conclusions

This study attempts to develop a consensus scenario for the CO_2-induced hydrologic changes based upon the results from climate models with both idealized and realistic geography. One of the significant changes identified here is the CO_2-induced reduction of zonal mean soil moisture in summer over two separate zones in middle and high latitudes. This reduction was noted in the earlier studies of Manabe and Stouffer (1980) and Wetherald and Manabe (1981) and is the main topic of the present study.

According to the zonal mean budget of soil moisture in high latitudes of both the sector- and the global models, the snowmelt season in the 4 x CO_2-experiment ends earlier than the corresponding season in the standard experiment. Thus, the warm season of rapid soil moisture depletion begins earlier due to enhanced evaporation resulting in less soil moisture during summer in the 4 x CO_2-experiment. The mechanism described above is mainly responsible for the CO_2-induced dryness during summer in high latitudes of these models.

In middle latitudes, a smaller snowmelt rate and stronger evaporation are also responsible for the faster reduction of soil moisture in late spring in the 4 x CO_2-experiment as compared with the standard experiment. This smaller rate of snowmelt in late spring results not only from the earlier occurrence of the snowmelt season discussed in the preceding paragraph, but also from the smaller total snow accumulation in middle latitudes where the surface air temperature is near the freezing point during winter.

In addition, one can identify another important factor which maintains the CO_2-induced dryness of soil moisture during summer in middle latitudes. As the season progress from winter to summer, the middle latitude rainbelt of a given model shifts polewards in both the 4 x CO_2- and the standard experiments. Generally, the middle latitude rainbelt in the 4 x CO_2-experiment is placed poleward of the corresponding rainbelt in the standard experiment partly due to the penetration of warm moisture rich air into higher latitudes. This implies that, in middle latitudes, the spring maximum of rainfall rate in the 4 x CO_2-experiment arrives earlier than the corresponding maximum in the standard experiment. Thus, the spring to summer reduction of rainfall rate begins earlier and helps maintain dryer soil during summer in the 4 x CO_2-experiment.

The earlier occurrence of the spring to summer reduction of rainfall rate mentioned above also results from the earlier beginning of the summer period of weak cyclone activity in the 4 x CO_2-experiment. Because of the CO_2-induced reduction of the meridional temperature gradient in the lower model troposphere, the summer period of weak atmos-

pheric disturbances in the 4 x CO_2-experiment begins earlier and lasts longer than in the standard experiment.

One of the important consequences of the CO_2-induced summer dryness is the suppression of evaporative heat loss from the continental surface. Thus, a larger fraction of radiative heat energy received by the continental surface has to be removed through an increased upward flux of sensible heat necessitating the warming of the continental surface in the regions of soil moisture reduction in summer.

According to the Student *t* analysis performed on the results from the sector model, the CO_2-induced summer dryness in middle and high latitudes is statistically significant at the 90% (or higher) confidence level. Other statistically significant changes of hydrologic variables include large increases in both soil moisture and runoff rate in high latitudes during most of a yearly cycle with the exception of the summer season. The penetration of moisture-rich, warm air into high latitudes is responsible for these increases.

Although the model experiments indicate notable soil moisture changes in both the subtropics and tropics, they vary considerably from one experiment to another. This is partly because the standard deviation of the temporal fluctuation of the time averaged soil moisture is larger than the CO_2-induced signal. It is therefore necessary to extend the period of time integration in each experiment substantially before one can establish statistical significance of these changes in soil moisture in lower latitudes.

Similar comments apply to the geographical distributions of the CO_2-induced changes of soil moisture. The distributions of soil moisture differences for the three models show a general reduction of soil moisture over both middle and high latitudes during the summer season. These tendencies are consistent with the zonal mean soil moisture differences discussed previously. However, the local details of these geographical differences vary from one model to another.

Acknowledgments

The authors are grateful to Y. Hayashi for valuable advice on the statistical evaluation of the results. Thanks are due to J. D. Mahlman, T. C. Yeh, S. L. Thompson, and S. H. Schneider for their constructive comments on a preliminary version of the manuscript. The authors would like to thank J. Kennedy, P. Tunison, J. Connor, M. Zadworny, and W. Ellis for their efficient and prompt assistance in the preparation of the manuscript and figures.

Appendix I: CO_2-induced Hydrologic Change in Annual Mean Climate

Although the seasonal variation of the CO_2-induced change of the hydrology is the main topic of this study, it is useful to review briefly the annual mean change. Figure A1a illustrates the latitudinal distributions of the rates of zonal mean precipitation and evaporation from both the 4 x CO_2- and standard experiments with the S15-model. The corresponding distributions from the G21-model is shown in Figure A1b. (For the distributions from the G15 model, refer to the paper by Manabe and Stouffer, 1980.) These

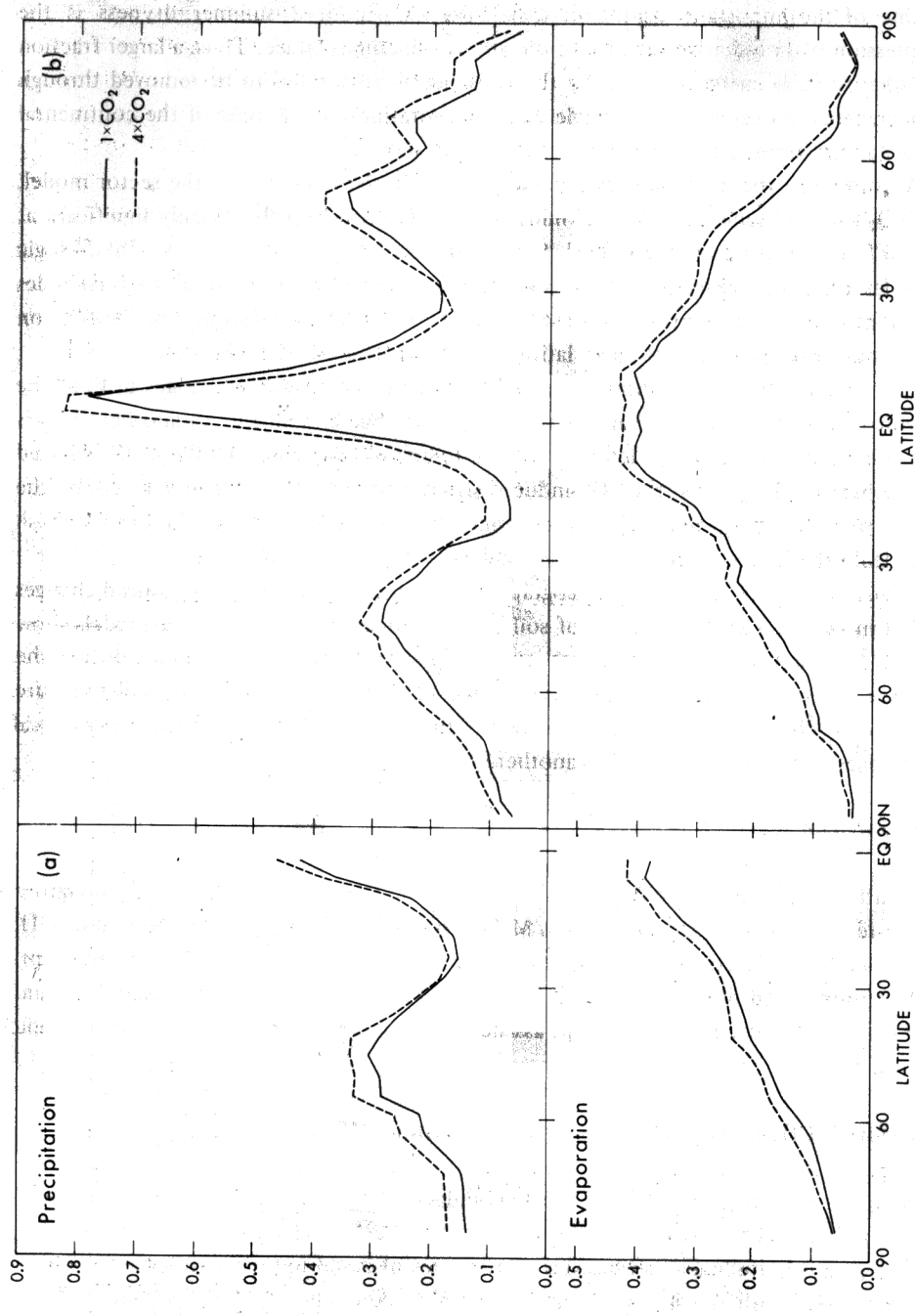

Fig. A1. Latitudinal distribution of the rates of zonal mean precipitation and evaporation from both the 4 x CO_2- and the standard experiments for the (a) S15 model and (b) G21 model. Units are in cm/day.

figures indicate that the area mean rates of both precipitation and evaporation increase in response to the increase of atmospheric CO_2-concentration as discussed by Manabe and Stouffer (1980). (Also see Wetherald and Manabe (1975) for an extensive discussion of this topic using the sector model results.) It is significant that the CO_2-induced increase in zonal mean precipitation rate is significantly larger than the corresponding increase of zonal mean evaporation rate in high latitudes. This is because the poleward transport of moisture increases markedly resulting from the general CO_2-induced warming of the atmosphere as discussed by Manabe and Wetheral (1980).

Figure A2 illustrates the latitudinal distributions of the zonal mean differences in various components of the soil moisture budget over continents between the 4 x CO_2- and the standard experiments. The distribution from the S15 model is shown in Figure A2a, whereas the results from the G15 and the G21 model are averaged with each other and are shown in Figure A2b. The differences considered here are $\Delta[\bar{r}]$, $\Delta[\bar{m}]$, $-\Delta[\bar{e}]$, and $-\Delta[\bar{f}]$. (See formula (7) in Section 4 for the balance requirement among these differences.)

This figure indicates that $\Delta[\bar{r}]$ has a large positive value in middle and high latitudes. This difference results from the increase in the poleward transport of moisture as discussed in the preceding paragraph. $\Delta[\bar{r}]$ is also positive over the equatorial region due to the increase in the equatorward moisture transport from the subtropics.

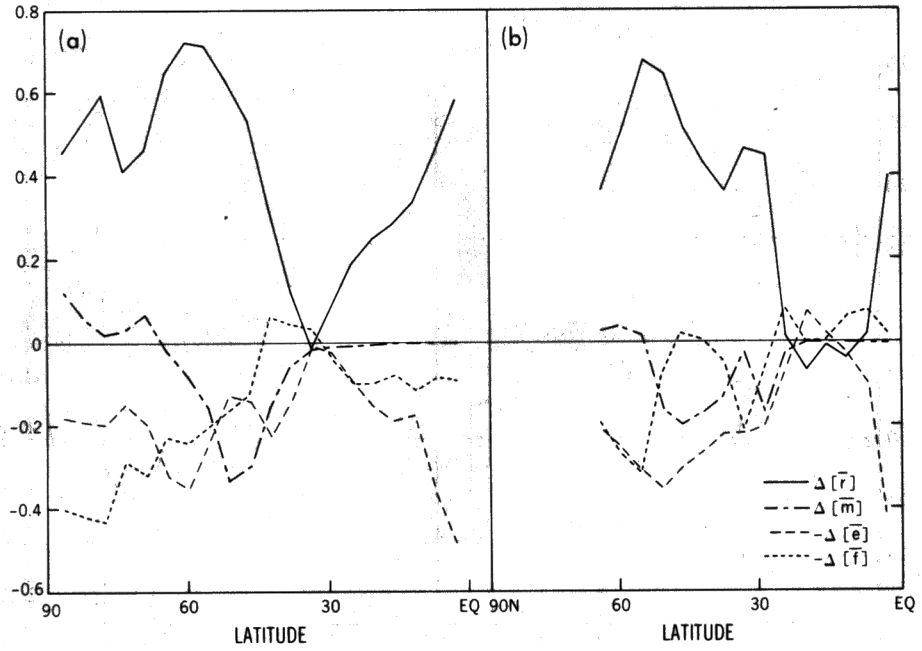

Fig. A2. Latitudinal distribution of the difference in the various components of the zonal mean soil moisture budget between the 4 x CO_2- and the standard experiment with the (a) S15 model and (b) the global models (the results from the two global models are averaged). Symbols have the same meaning here as in Figure 12. Units are in cm/day. The results from the global models are not shown for the entire Southern Hemisphere and high latitudes of the Northern Hemisphere because most of these areas are occupied by oceans or continental icesheets.

In high latitudes where the surface air temperature is below the freezing point during most of a year, the CO_2-induced increase in precipitation implies an increase of snowfall. Accordingly, the amount of snow available for melting in the 4 x CO_2-experiment is larger than the corresponding amount in the standard experiment. This is why $\Delta[\bar{m}]$ has small positive values in high latitudes of all three models. However, $\Delta[\bar{m}]$ is negative in middle latitudes where the surface air temperature is near the freezing point in winter. Due to the CO_2-induced warming of surface air temperature, a larger fraction of precipitation is rainfall in middle latitudes for the 4 x CO_2-experiment as compared with the standard experiment. Thus, a smaller amount of snow is available for melting in this zone.

Because of the CO_2-enhancement of evaporation, $-\Delta[\bar{e}]$ is negative at most latitudes except over the subtropics where the evaporation rate is small in both experiments.

The latitudinal distribution of $\Delta[\bar{w}]$ for the S15 model and that of the average $\Delta[\bar{w}]$ for the two global models are shown in Figure A3. For assessment of statistical significance of the result, the confidence interval defined in Section 4 is added to the distribution from the S15 model. In general, $\Delta[\bar{w}]$ is positive in high latitudes and the equatorial region, but is negative in middle latitudes and subtropics. An examination of the confidence interval for the S15 model results indicates that the sign of $\Delta[\bar{w}]$ in low latitudes is less significant statistically than the sign of the differences in higher latitudes. For

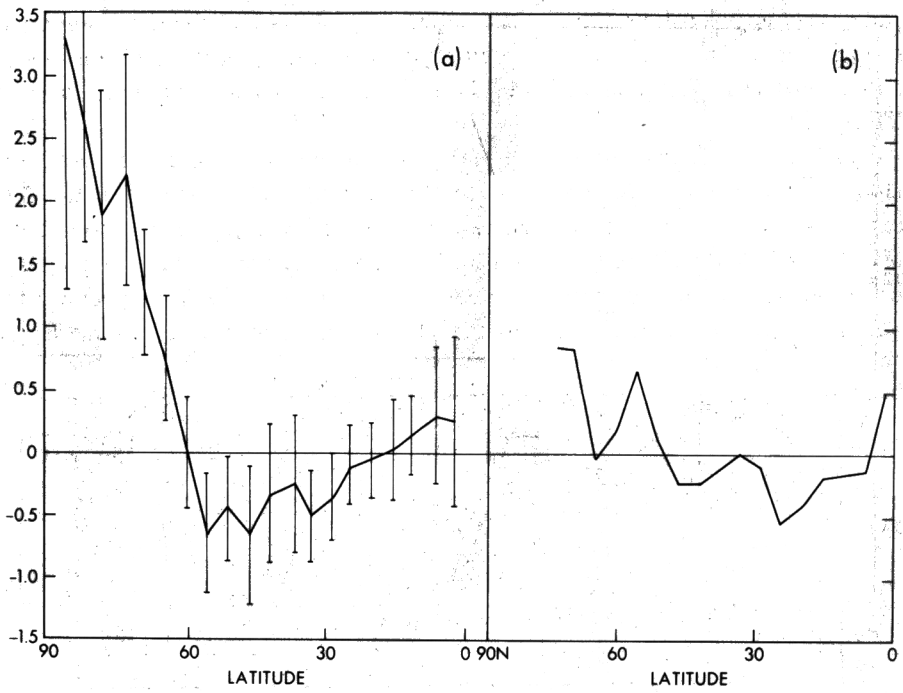

Fig. A3. Latitudinal distribution of the annual mean difference of zonal mean soil moisture between the 4 x CO_2 and the standard experiment. (a) S15 model. (b) the average of the G15 and G21 models. The vertical line segments in the S15 model distribution represent the 90% confidence intervals. Units are in cm. Note that there is a decimal point between the two digits of each number on the ordinate.

further discussion of the CO_2-induced annual mean change of soil moisture, (see Manabe and Wetherald (1980), Manabe and Stouffer (1980) and Wetherald and Manabe (1981)).

Appendix II: Kinetic Energy of Transient Disturbances

It is expected that the activity of transient disturbances in the atmosphere strongly influences the global distribution of precipitation rate and accordingly those of soil moisture and other hydrologic variables. Therefore, it is worthwhile to briefly describe the CO_2-induced change in the distribution of kinetic energy of transient eddies in the S15 model atmosphere.

Figure A4 illustrates the latitude-height distribution of zonally averaged, monthly mean kinetic energy of transient disturbances in the S15 model atmosphere for the month of January. The Northern and Southern Hemispheric portions of the figure are indicative of the winter and summer distributions, respectively. Here, the zonally averaged, monthly mean kinetic energy of transient eddies TKE is defined as follows

$$\mathrm{TKE} = (1/2) \cdot \overline{[(u - \bar{u}^{m})^2 + (v - \bar{v}^{m})^2]}^{m}$$

where u and v are the zonal and meridional wind, respectively, and $^{-m}$ and [ ] indicate monthly mean and zonal mean operators, respectively. (Note that the definition of the notation [ ] used here differs from the definition used in the preceding sections. In this equation, zonal average is computed over the entire latitude circle rather than the continental region.)

According to Figure A4, the kinetic energy of transient disturbances reduces below the 300 mb level and increases above this level in response to the increase of the CO_2-concentration. Qualitatively similar changes in transient eddy kinetic energy were noted by Manabe and Wetherald (1975) in their CO_2-climate sensitivity study employing a sector model with an annual mean insolation. They attributed the tropospheric reduction of transient eddy kinetic energy to the CO_2-induced reduction of the meridional

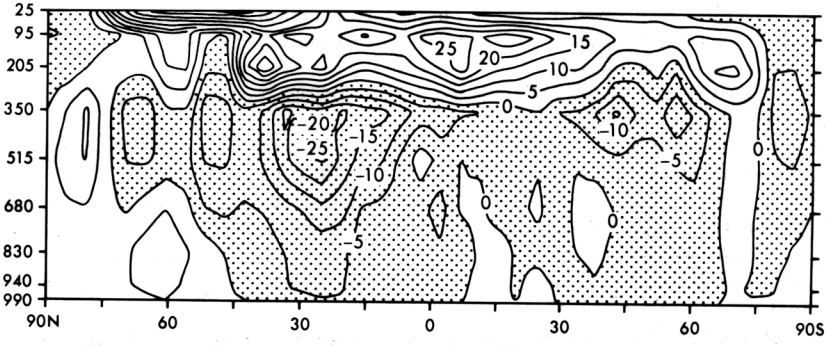

Fig. A4. Latitude-height distribution of zonally averaged difference of kinetic energy of transient disturbances between the 4 x CO_2 and the standard experiments with the S15 model for the month of January. Units are in 10^4 cm^2 s^{-2}. The units of the ordinate are mb.

temperature gradient below the 350 mb level. On the other hand, they speculated that the increase in the upper layer is due to the increase in the meridional temperature gradient and the reduction of static stability above the 350 mb level of their model. Further study is required in order to elucidate the specific dynamical mechanisms responsible for the change of transient eddy kinetic energy described above.

Figures A5a and b illustrate the latitudinal and seasonal variation of zonally averaged, monthly mean kinetic energy of transient disturbances at the 350 mb level of the S15 model atmosphere from the standard and 4 x CO_2-experiments, respectively. In addition, the corresponding variation of the difference in the kinetic energy between the two experiments is shown in Figure A5c. This figure clearly indicates that the reduction in the kinetic energy of transient eddies is particularly pronounced in early spring and fall. Accordingly, the summer period of relatively low eddy kinetic energy becomes longer in response to the increase in CO_2-concentration. As discussed in Section 4, the earlier timing of the spring maximum in the precipitation rate partly results from the earlier beginning of the summer period of weak wave activity.

References

Bourke, W.: 1974, 'A Multi-level Model. I. Formulation and Hemispheric Integrations', *Monthly Weather Rev.* **102**, 688.

Bryan, K.: 1969, 'Climate and the Ocean Circulation: III. The Ocean Model', *Monthly Weather Rev.* **97**, 806.

Chervin, R. M. and Schneider, S. H.: 1976, 'On Determining the Statistical Significance of Climate Experiments with General Circulation Models', *J. Atmos. Sci.* **33**, 405.

Gordon, T. and Stern, B.: 1974, 'The GARP Programme on Numerical Experimentation', Report No. 7, 46.

Hayashi, Y.: 1982, 'Confidence Intervals of a Climatic Signal', Submitted to *J. Atmos. Sci.*

Hering, W. S. and Borden, T.R. Jr.: 1965, 'Mean Distribution of Ozone Density over North America', 1963–1964. Environmental Research Papers, No. 162, U.S. Air Force Cambridge Research Lab., Hanscom Field, Mass., 19 pp.

Hoskins, J. J. and Simmons, A. J.: 1975, 'A Multi-Layer Spectral Model and the Semi-Implicit Method', *Quart. J. Roy. Meteor. Soc.* **104**, 91.

Lacis, A. A. and Hansen, J. E.: 1974, 'A Parameterization for the Absorption of Solar Radiation in the Earth's Atmosphere', *J. Atmos. Sci.* **31**, 118.

Lvovitch, M. I. and Ovtchinnikov, S. P.: 1964, 'Physical-Geographical Atlas of the World (in Russian)', Academy of Sciences, U.S.S.R., and Department of Geodesy and Cartography, State Geodetic Commission, Moscow. (See p. 61).

Manabe, S.: 1969a, 'Climate and Ocean Circulation. I. The Atmospheric Circulation and the Hydrology of the Earth's Surface'. *Monthly Weather Rev.* **97**, 739.

Manabe, S. and Holloway, J. L. Jr.: 1975, 'The Seasonal Variation of the Hydrologic Cycle as Simulated by a Global Model of the Atmosphere', *J. Geophys. Res.* **80**, 1617.

Manabe, S., Hahn, D. G., and Holloway, J. L.: 1979, 'Climate Simulation with GFDL Spectral Models of the Atmosphere', GARP Publication Series No. 22, Vol. 1, 41–94. World Meteorological Organization, Geneva, Switzerland.

Manabe, S. and Stouffer, R. J.: 1979, 'A CO_2-Climate Sensitivity Study with a Mathematical Model of the Global Climate', *Nature* **282**, 491.

Manabe, S. and Stouffer, R. J.: 1980, 'Sensitivity of a Global Climate Model to an Increase of CO_2-concentration in the Atmosphere', *J. Geophys. Res.* **85**, 5529.

Manabe, S., Smagorinsky, J., and Strickler, R. F.: 1965, 'Simulated Climatology of a General Circulation Model with a Hydrologic Cycle', *Monthly Weather Rev.* **93**, 769.

Manabe, S. and Wetherald, R. T.: 1975, 'The Effects of Doubling the CO_2-Concentration on the Climate of a General Circulation Model', *J. Atmos. Sci.* **32**, 3.

Manabe, S. and Wetherald, R. T.: 1980, 'On the Distribution of Climate Change Resulting from an Increase in CO_2-Content of the Atmosphere', *J. Atmos. Sci.* **37**, 99.

Möller, F.: 1951, 'Quarterly Charts of Rainfall for the Whole Earth', (in German), *Petermanns. Geograph. Mitt.* **95**, 1.

Orsag, S. A.: 1970, 'Transform Method for Calculation of Vector-Coupled Sums: Application to the Spectral form of the Vorticity Equation', *J. Atmos. Sci.* **27**, 890.

Panofsky, H. A. and Brier, G. W.: 1965, 'Some Applications of Statistics to Meteorology', The Pennsylvania State University, State College, Pa.

Posey, J. W. and Clapp, P. F.: 1964, 'Global Distribution of Normal Surface Albedo', *Geofisica Internationale* **4**, 33.

Rodgers, C. D. and Walshaw, C. D.: 1966, 'The Computation of Infrared Cooling Rate in Planetary Atmospheres', *Quart. J. Roy. Met. Soc.* **92**, 67.

Sasamori, T., London, J., and Hoyt, D. V.: 1972, 'Radiation Budget of Southern Hemisphere', *Meteorological Monographs*, Vol. **13**, No. 35, (Meteorology of the Southern Hemisphere, by C. W. Newton (ed.)), American Meteorological Society, Boston, Mass.

Stone, H. M. and Manabe, S.: 1968, 'Comparison Among Various Numerical Models Designed for Computing Infrared Cooling', *Monthly Weather Rev.* **96**, 735.

Wetherald, R. T. and Manabe, S.: 1975, 'The Effects of Changing the Solar Constant on the Climate of a General Circulation Model', *J. Atmos. Sci.* **32**, 2044.

Wetherald, R. T. and Manabe, S.: 1981, 'Influence of Seasonal Variation upon the Sensitivity of a Model Climate', *J. Geophys. Res.* **86**, 1194.

(Received 31 July, 1981; in revised form 3 September, 1981).

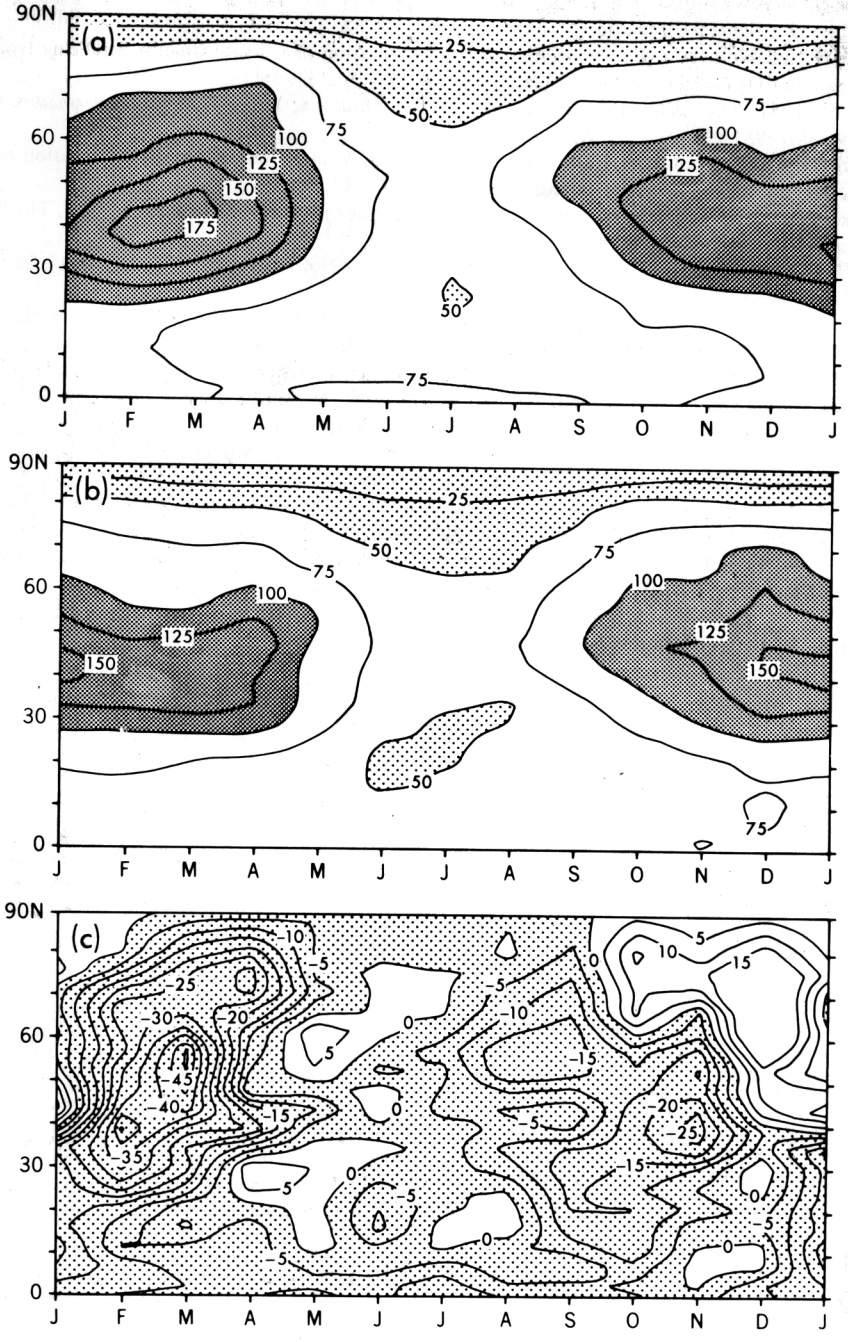

Fig. A5. The latitudinal and seasonal variation of zonal mean kinetic energy of transient disturbances at the 350 mb level of the S15 model for (a) the standard experiment, (b) the 4 x CO_2 experiment and (c) the difference between the 4 x CO_2 and the standard experiments. Units are in 10^4 cm^2 s^{-2}.